Atmos. Meas. Tech. Discuss., 7, 5173–5221, 2014
www.atmos-meas-tech-discuss.net/7/5173/2014/
doi:10.5194/amtd-7-5173-2014

Atmospheric Measurement Techniques Discussions
Open Access

Fine and coarse dust separation with polarization lidar

R. E. Mamouri[1] **and A. Ansmann**[2]

[1]Cyprus University of Technology, Dep. of Civil Engineering and Geomatics, Limassol, Cyprus
[2]Leibniz Institute for Tropospheric Research, Leipzig, Germany

Received: 21 April 2014 – Accepted: 14 May 2014 – Published: 23 May 2014

Correspondence to: R. E. Mamouri (rodanthi.mamouri@cut.ac.cy)

Published by Copernicus Publications on behalf of the European Geosciences Union.

Abstract

The polarization-lidar photometer networking (POLIPHON) method for separating dust and non-dust aerosol backscatter and extinction, volume, and mass concentration is extended to allow for a height-resolved separation of fine-mode and coarse-mode dust properties in addition. The method is applied to a period with complex aerosol layering of fine-mode background dust from Turkey and Arabian desert dust from Syria. The observation was performed at the combined European Aerosol Research Lidar Network (EARLINET) and Aerosol Robotic Network (AERONET) site of Limassol (34.7° N, 33° E), Cyprus, in September 2011. The dust profiling methodology and case studies are presented. Consistency between the column-integrated optical properties obtained with sun/sky photometer and the respective results derived by means of the new lidar-based method corroborate the applicability of the extended POLIPHON version.

1 Introduction

Mineral dust belongs to the major components of the atmospheric aerosol system and sensitively influences climatic and environmental conditions. The deserts in northern Africa and in the Middle East (western Asia) are major dust sources and have a strong impact on air quality and aerosol conditions in southern and eastern Europe. Large amounts of mineral dust can be advected over long distances in the lower free troposphere from the deserts to remote areas within few days (Ansmann et al., 2003; Papayannis et al., 2008; Baars et al., 2011). Turbulent exchange processes at the interface between the free troposphere and the planetary boundary layer leads to efficient downard mixing of dust towards the surface. Emissions from arid (non-desert) and semi-arid regions and areas with strong agricultural activities also contribute to the dust load over Europe.

For a proper consideration of mineral dust in climate modelling and air quality monitoring efforts, vertical profiling of dust with the potential to distinguish between

AMTD
7, 5173–5221, 2014

fine-mode and coarse-mode dust is requested (Kok, 2011; Zhang et al., 2013). Fine and coarse dust particles influence the Earth's radiation budget, cloud processes, and environmental conditions in a different way (Nabat et al., 2012; Mahowald et al., 2014). The optical properties and radiative impact are widely controlled by coarse-mode dust particles. However, 20–25 % of the dust-related optical depth is caused by fine-mode dust according to Aerosol Robotic Network (AERONET) sun/sky photometer oberservations (see Sect. 3). Regarding the influence on cloud processes, coarse dust particles belong to the most favorable cloud condensation and ice nuclei (DeMott et al., 2010). Fine-mode dust particles, on the other hand side, can have a significant impact on air quality, defined in PM (particulate matter) aerosol levels and even may sometimes dominate $PM_{1.0}$ (particles with diameters < 1.0 µm) observation at sites close to deserts such as Cyprus. As an example, on 1 April 2013 the 500 nm aerosol particle optical thickness (AOT) increased from 1 to 4 between 08:00 and 12:00 UTC over Cyprus during a rather strong Saharan dust outbreak. These large AOT values indicate fine-mode dust mass concentrations of 35–140 $\mu g\,m^{-3}$ in the tropospheric column up to 4–5 km height which is 10–15 % of the total dust mass concentration.

In this contribution we present to our knowledge the first attempt to use empirical knowledge on the light depolarizing properties of fine-mode and coarse-mode dust (Sakai et al., 2010) in the interpretation of polarization lidar observations with the goal to separate fine-mode dust, coarse-mode dust, and remaining non-dust aerosol components. So far, polarization lidars are used to identify dust and to separate backscatter and extinction coefficients of dust and non-dust aerosol (e.g., Sugimoto and Lee, 2006; Nishizawa et al., 2007; Tesche et al., 2009, 2011; Groß et al., 2011; Ansmann et al., 2011a, 2012). The most important parameter in these studies is the so-called particle linear depolarization ratio. The laser transmits linearly polarized laser pulses and the receiving unit detects the parallel- and cross-polarized signal components with respect to the plane of laser polarization. The ratio of calibrated cross-polarized to parallel-polarized signal yields the volume linear depolarization ratio from which the particle depolarization ratio can be computed (e.g., Tesche et al., 2009).

Our attempt to develop a method for fine and coarse dust separation was motivated by observations of enhanced levels of free tropospheric depolarization ratios of 10–20 % with the European Aerosol Research Lidar Network (EARLINET) polarization lidar over Limassol (34.7° N, 33° E), Cyprus, indicating the presence of dust, and at the same time, AERONET sun/sky photometer measurements indicating the absence of continental coarse-mode dust particles. These enhanced depolarization ratios were thus most likely exclusively caused by fine-mode dust particles. According to laboratory studies of Sakai et al. (2010) for a laser wavelength of 532 nm, dust particle size distributions dominated by fine-mode particles (mostly with diameters $< 1\,\mu m$) cause particle depolarization ratios around 0.15 ± 0.05, whereas particle depolarization ratios of 0.39 ± 0.04 were observed in the presence of a high number of desert dust particles in the super micrometer range (coarse-mode particles). These findings are supported by modelling studies for irregularly shaped particles (Gasteiger et al., 2011) and also consistent with field observations close to the Sahara (Freudenthaler et al., 2009; Groß et al., 2011). In these field studies, pure dust depolarization ratio ranged from 30–35 % at 532 nm. These values can be reproduced with fine and coarse dust depolarization ratios of 16 % and 39 % when assuming a fine-mode contribution to the total dust particle backscatter coefficient of about 25 %, a similar percentage as mentioned above for the fine-mode AOT contribution to the total AOT.

Presently several new dust profiling methods are tested which built on existing AERONET and EARLINET infrastructures in Europe. Two fundamentally different lidar/photometer-based retrieval concepts are applied, the Lidar/Radiometer Inversion Code (LIRIC) (Chaikovsky et al., 2012) and Generalized Aerosol Retrieval from Radiometer and Lidar Combined Data (GARRLiC) methods (Lopatin et al., 2013) and, as an alternative technique, the Polarization Lidar Photometer Networking (POLIPHON) approach (Ansmann et al., 2012). LIRIC uses profiles of elastic-backscatter lidar return signals at 355, 532, and 1064 nm and, as a priori assumptions, AERONET photometer retrieval products (column-integrated particle size distributions, composition, complex refractive index, and particle shape). The method is based on a particle shape model. The irregularly shaped dust particles are assumed to be spheroidal dust particles. This approach works well in the case of the analysis of pure sun/sky photometer data (Dubovik et al., 2006). However, it is shown by Wagner et al. (2013) that this particle shape model introduces significant uncertainties in the LIRIC aerosol products when applied to lidar backscatter returns, i.e., to light scattering information for a scattering angle of exactly 180°. Products of the LIRIC data analysis are height profiles of particle backscatter and extinction coefficients at the three wavelengths, and particle volume and mass concentration profiles separately for fine-mode and coarse-mode particles. GARRLiC is an extended version of LIRIC and pursues an even deeper synergy of lidar and radiometer data in the retrievals. To apply the LIRIC and GARRLiC methods, lidar and photometer observation have to be performed simultaneously. Thus, cloudfree conditions are required.

In contrast, the POLIPHON approach is designed to explicitly avoid the use of a particles shape model and also a strong dependence on photometer observations. POLIPHON is applicable even at cloudy conditions which often occur during dust outbreaks. The technique is based on measured 180° light-depolarization characteristics for dust aerosol particles. This approach, originally developed for the separation of non-dust and dust fractions (here denoted as one-step POLIPHON method) is extended to allow even a separation of fine-mode dust from coarse-mode dust (two-step POLIPHON technique). The comparably simple and robust method for the retrieval of optical properties, volume, and mass concentrations is outlined in Sect. 4. POLIPHON belongs to the family of well established lidar aerosol-typing methods which built on empirically gathered optical aerosol properties. Examples of observations and applications are presented by Groß et al. (2013) and Burton et al. (2014).

In Sect. 2, the lidar and photometer instruments are briefly described. Section 3 presents an overview of typical optical properties of desert dust in terms of fine-mode and coarse-mode dust characteristics to emphasize the need for the development of more sophisticated fine and coarse dust separation techniques. The extended two-step POLIPHON methodology is outlined in Sect. 4. The new retrieval scheme is then

AMTD
7, 5173–5221, 2014

applied to an episode with complex aerosol layering with background fine-mode dust as well as desert dust (coarse and fine dust) during a strong dust outbreak in September 2011 (Sect. 5). Summarizing and concluding remarks are given in Sect. 6.

2 Instrumentation

2.1 Polarization lidar

The lidar station of the Cyprus University of Technology (CUT) at Limassol (34.7° N, 33° E, 50 m a.s.l.) is located about 150 km south of Turkey and 400 km west of Syria (Mamouri et al., 2013). The lidar has four channels for the measurement of elastic-backscatter signals at 532 and 1064 nm, the nitrogen Raman signal at 607 nm. The lidar transmits linearly polarized laser pulses at 532 nm and detects the parallel- and cross-polarized signal components at this wavelength. Calibration of the polarization channels is performed by rotating the box with the polarization sensitive channels following the methodology of Freudenthaler et al. (2009). The transmission properties of the receiver (for parallel and perpendicularly polarized light) required for an accurate determination of the particle linear depolarization ratio are known from measurements.

The full overlap of the laser beam with the receiver field of view of the 20 cm Cassegrain telescope is obtained at heights around 300 m a.s.l. The overlap characteristics was checked by Raman lidar observations at 532 and 607 nm (nitrogen Raman channel, Wandinger and Ansmann, 2002) at clear sky conditions at Limassol. The measured volume depolarization ratio is reliable to about 50 m above ground. Overlap effects widely cancel here because the depolarization ratio is calculated from the ratio of the cross-polarized to the parallel-polarized signal component (Freudenthaler et al., 2009).

In this paper, we will make use of the determined particle backscatter coefficient and the particle depolarization ratio at 532 nm. The determination of the particle backscatter coefficient is described by Mamouri et al. (2013). For the calibration of the profile

AMTD
7, 5173–5221, 2014

of the measured 532 nm elastic backscatter signal, pure Rayleigh signals are simulated based on actual temperature and pressure profiles from numerical weather forecast data or actual nearby radiosonde observations. The measured 532 nm signals are then fitted to the Rayleigh signal profile in the aerosol-free middle to upper troposphere. The corresponding reference particle backscatter coefficient was set to zero at heights above 4–5 km in the particle backscatter retrieval after Sasano et al. (1985). The particle depolarization ratio is computed from the volume depolarization ratio by means of the determined particle backscatter coefficient (Freudenthaler et al., 2009). Uncertainties in the retrieval products are discussed by Mamouri et al. (2013) and are typically of the order of 10 %.

2.2 Sun/sky photometer

The lidar is collocated with a sun/sky photometer of the Aerosol Robotic Network (AERONET, CUT–TEPAK site, Limassol, Cyprus, http://aeronet.gsfc.nasa.gov) (Holben et al., 1998). The CUT AERONET photometer allows the retrieval of the aerosol optical thickness (AOT) at eight wavelengths from 339 to 1638 nm. Sky radiance observations at four wavelengths complete the AERONET observations. From the spectral AOT distribution, the Ångström exponent AE (Ångström, 1964), the fine mode fraction FMF (fraction of fine-mode AOT to total AOT) (O'Neill et al., 2003), the sphericty parameter SMF (fraction of spherical particle volume concentration to total particle volume concentration), and the column lidar ratio S_{col} are retrieved. AOT errors are of the order of 0.01–0.02.

3 Fine- and coarse-mode optical properties of mineral dust observed with AERONET photometers

Before presenting the new two-step POLIPHON approach, we want to discuss the fine-mode dust impact on the overall dust optical and microphyisical properties and to

AMTD
7, 5173–5221, 2014

provide in this way convincing arguments that the development of lidar methods which allow to discriminate fine dust and coarse dust profiles is a useful attempt and delivers interesting data for atmospheric and evnvironmental research. The first example, shown in Fig. 1, is a major Saharan dust outbreak reaching Cyprus on 1 April 2013. According to Fig. 2, the 500 nm AOT increased from 1–4 within four hours (08:00–12:00 UTC). Disregarding the rather strong AOT increase, the fine-mode fraction remained almost constant. About 25 % of the 500 nm optical depth was caused by fine-mode dust.

Figure 3 gives an overview of the dust observations with an AERONET photometer during the Saharan Mineral Dust Experiment 1 (SAMUM-1) (Heintzenberg, 2009; Ansmann et al., 2011b) in terms of 500 nm AOT, AE, FMF, and FVF. The SAMUM-1 field site of Ouarzazate, Morocco, is very close to the Sahara with a minimum impact of non-dust aerosol components on the photometer observations. Two pronounced dust outbreaks from Algeria are indicated in Fig. 3. Figure 4 shows two dust particle size distributions measured within the two SAMUM-1 dust outbreak periods. During these specific periods the FMF values are 0.24–0.35 and again indicate a significant influence of fine-mode dust on the measured optical properties. The fine-mode volume fraction ranges from 10 % to 15 %. These two observational cases corroborate that a lidar-based separation of fine and coarse dust profiles in terms of optical and microphysical properties is a useful addition to atmospheric profiling techniques.

In the discussion and interpretation of our observations in Sect. 4, we need characteristic values for the dust Ångström exponent, separately for fine mode and coarse mode. As can be seen from Figs. 3 and 4, fine-mode dust AE is about 1.5 ± 0.1, and coarse-mode AE is close to -0.2 ± 0.05. In addition, we need particle extinction-to-volume conversion factors to translate lidar-derived profiles of the dust extinction coefficient into volume and mass concentrations. In Fig. 4, these conversion factors (v_f/AOT_f, v_c/AOT_c) are computed from the retrieved AERONET values of the column-integrated particle volume concentrations (v_f, v_c) for fine-mode dust and coarse-mode dust, respectively, and corresponding particle optical depths (500 nm AOT_f, AOT_c).

The SAMUM-1 conversion factors in Fig. 4 are in good agreement with simulations of Barnaba and Gobbi (2004). Based on several thousands of realistic combinations of particle number concentration, size distribution, and refractive index characteristics, the volume-to-extinction ratio for dust size distributions dominated by supermicron dust particles typically ranges from 0.6–0.9 × 10^{-6} m for 532 nm wavelength. The maximum value is 1.0 × 10^{-6} m for very large dust particles. For submicron-dust-dominated particle ensembles, the conversion factors are between 0.25 × 10^{-6} m and 0.4 × 10^{-6} m.

4 Two-step POLIPHON method

4.1 Theoretical background

The new two-step POLIPHON method uses the same separation technique as the one-step approach. The latter method is described in detail by Tesche et al. (2009) for a two-aerosol component mixture of desert dust and biomass burning smoke. We briefly introduce the one-step approach and use the notation of Tesche et al. (2009).

The procedure to separate dust-related and smoke-related (or more general non-dust-related) profiles of backscattering starts from the equation for the particle depolarization ratio

$$\delta_\mathrm{p} = \frac{\beta_\mathrm{nd}^\perp + \beta_\mathrm{d}^\perp}{\beta_\mathrm{nd}^\parallel + \beta_\mathrm{d}^\parallel}. \quad (1)$$

$\beta^\perp$ and $\beta^\parallel$ are so-called cross and parallel-polarized particle backscatter coefficients which can in principle be computed from the lidar return signals detected with the cross-polarized and parallel-polarized signal channels. The indices d and nd denote dust and non-dust aerosol components, respectively. The sum of all four backscatter contributions in Eq. (1) yields the total particle backscatter coefficient β_p. The overall particle backscatter coefficient β_p is calculated in the way described in Sect. 2.1.

AMTD
7, 5173–5221, 2014
Fine and coarse dust profiling
R. E. Mamouri and A. Ansmann

As shown by Tesche et al. (2009) the particle depolarization ratio can be expressed by

$$\delta_p = \frac{\beta_{nd}\delta_{nd}(1+\delta_d) + \beta_d\delta_d(1+\delta_{nd})}{\beta_{nd}(1+\delta_d) + \beta_d(1+\delta_{nd})} \quad (2)$$

with the dust and non-dust depolarization ratios δ_d and δ_{nd}, respectively. After substituting β_{nd} by $\beta_p - \beta_d$, we solve the resulting equations to obtain a solution for β_d:

$$\beta_d = \beta_p \frac{(\delta_p - \delta_{nd})(1+\delta_d)}{(\delta_d - \delta_{nd})(1+\delta_p)} \qquad \text{for } \delta_p > \delta_{nd}\,, \quad (3)$$

$$\beta_d = 0 \qquad \text{for } \delta_p \le \delta_{nd}\,. \quad (4)$$

The non-dust particle backscatter coefficient is then obtained from $\beta_p - \beta_d$.

In the computation after Eqs. (1)–(3) we need to estimate the non-dust depolarization ratio δ_{nd} and the dust depolarization ratio δ_d. The particle depolarization ratio for Saharan dust of $\delta_d = 0.31 \pm 0.03$ (Freudenthaler et al., 2009; Groß et al., 2011) is in good agreement with the one for Asian dust (Sugimoto et al., 2003; Shimizu et al., 2004). The non-dust-related depolarization ratio δ_{nd} may vary from 0.015–0.15 according to the literature. The values accumulate around 0.05 according to published values (Murayama et al., 1999; Murayama et al., 2004; Fiebig et al., 2002; Sugimoto et al., 2003; Müller et al., 2005, 2007; Sugimoto and Lee, 2006; Chen et al., 2007; Heese and Wiegner, 2008).

In Fig. 5, the one-step and the two-step methods are illustrated. In our two-step approach we now introduce three types of aerosols: non-dust particles causing a particle linear depolarization ratio of $\delta_{nd} = 0.05$, fine-mode dust causing a depolarization ratio of $\delta_{df} = 0.16$, and coarse-mode desert dust causing a particle depolarization ratio of $\delta_{dc} = 0.39$. Our focus is on lofted free tropospheric aerosol. We assume the absence of coarse marine particles here so that spherical particles exclusively belong to the fine mode particle fraction.

AMTD
7, 5173–5221, 2014

R. E. Mamouri and A. Ansmann

The basic equation of our two-step retrieval scheme is

$$\delta_{\mathrm{p}} = \frac{\beta_{\mathrm{nd}}^{\perp} + \beta_{\mathrm{df}}^{\perp} + \beta_{\mathrm{dc}}^{\perp}}{\beta_{\mathrm{nd}}^{\parallel} + \beta_{\mathrm{df}}^{\parallel} + \beta_{\mathrm{dc}}^{\parallel}}. \tag{5}$$

In each of the two steps, two kinds of aerosols are separated (see Fig. 5). In the first round we start from

$$\delta_{\mathrm{p}} = \frac{\beta_{\mathrm{pf}}^{\perp} + \beta_{\mathrm{dc}}^{\perp}}{\beta_{\mathrm{pf}}^{\parallel} + \beta_{\mathrm{dc}}^{\parallel}}. \tag{6}$$

Index pf indicates fine-mode particles as a whole, i.e., spherical as well as non-spherical sub-micrometer particles with radii of ≤ 500 nm. Analog to the step from Eq. (1) to Eq. (3), here we obtain for the coarse dust backscatter coefficient

$$\beta_{\mathrm{dc}} = \beta_{\mathrm{p}} \frac{(\delta_{\mathrm{p}} - \delta_{\mathrm{pf,\,max}})(1 + \delta_{\mathrm{dc}})}{(\delta_{\mathrm{dc}} - \delta_{\mathrm{pf,\,max}})(1 + \delta_{\mathrm{p}})} \qquad \text{for } \delta_{\mathrm{p}} > \delta_{\mathrm{pf,\,max}}, \tag{7}$$

$$\beta_{\mathrm{dc}} = 0 \qquad \text{for } \delta_{\mathrm{p}} \leq \delta_{\mathrm{pf,\,max}}. \tag{8}$$

We assume $\delta_{\mathrm{pf,\,max}} = 0.12$ and $\delta_{\mathrm{dc}} = 0.39$ in Eq. (7) to determine the coarse-mode contribution β_{dc} to β_{p}. Such a fine-mode characterizing depolarization ratio of $\delta_{\mathrm{pf,\,max}} = 0.12$ instead of 0.16 for fine dust after Sakai et al. (2010) assumes that the fine-mode always includes a certain fraction (here about 25 %) of anthropogenic haze and/or biomass burning smoke. All δ_{p} values between $\delta_{\mathrm{pf,\,max}} = 0.12$ and $\delta_{\mathrm{dc}} = 0.39$ indicate mixtures of coarse dust and fine (spherical and non-sphericial) particles (see Fig. 5).

We recommend to generally assume a 25 % contribution of fine spherical particle to the overall fine-mode fraction (in the polluted Northern Hemisphere) when pronounced dust layers are detected and the two-step method is going to be applied. Even for strong desert dust outbreak plumes, $\delta_{\mathrm{pf,\,max}} = 0.16$ (assuming that only pure fine dust

AMTD
7, 5173–5221, 2014

R. E. Mamouri and A. Ansmann

Title Page
Abstract Introduction
Conclusions References
Tables Figures
◀◀ ▶▶
◀ ▶
Back Close
Full Screen / Esc
Printer-friendly Version
Interactive Discussion

contributes to FMF) in the first round is probably too large. During situations with traces of soil or desert dust in lofted aerosol layers, indicated by low depolarization ratios of about 0.05–0.10, the two-step method will only deliver backscatter coefficients for fine-mode particles when using $\delta_{\text{pf, max}} = 0.12$. Then, the solutions of the one-step and two-step methods may be compared. The range of fine and coarse dust profiles obtained with the two methods may be used as the range of possible solutions in terms of fine and coarse dust backscatter coefficients.

Before we can start the second round, i.e, the separation of fine spherical from fine non-spherical particles) we have to remove the optical effects of coarse-mode dust from the total particle backscatter coefficient and the particle depolarization ratio. The profile of the fine-mode-related backscatter coefficient is given by

$$\beta_{\text{pf}} = \beta_{\text{p}} - \beta_{\text{dc}}. \tag{9}$$

Regarding the removal of the coarse-mode depolarization effect, one may use Eq. (11) of Tesche et al. (2009), here in the form of

$$\delta_{\text{pf}} = \frac{\beta_{\text{dc}}(\delta_{\text{p}} - \delta_{\text{dc}}) + \beta_{\text{pf}}\delta_{\text{p}}(1 + \delta_{\text{dc}})}{\beta_{\text{dc}}(\delta_{\text{dc}} - \delta_{\text{p}}) + \beta_{\text{pf}}(1 + \delta_{\text{dc}})}. \tag{10}$$

However, it can be shown that solving of Eq. (10) is equivalent to the simple setting according to

$$\delta_{\text{pf}} = \delta_{\text{p}} \qquad \text{for } \delta_{\text{p}} \leq 0.12, \tag{11}$$

$$\delta_{\text{pf}} = 0.12 \qquad \text{for } \delta_{\text{p}} > 0.12 \tag{12}$$

in our case with $\delta_{\text{pf, max}} = 0.12$. The profile for δ_{pf} after Eqs. (11) and (12) corresponds to the fine-mode backscatter profile after Eq. (9). An example for the coarse-dust-corrected profiles of the particle backscatter coefficient and depolarization ratio is shown in Sect. 4.

In the second round, we set the maximum fine-mode dust depolarization ratio (upper boundary of possible fine-mode depolarization ratios) to $\delta_{df} = 0.16$ as suggested by Sakai et al. (2010). Since the maximum depolarization value is still assumed to be 0.12, the assumption implies again that the fine-mode dust fraction is of the order of 75 % and the residual part consists of haze and smoke particles.

The second round starts from

$$\delta_{pf} = \frac{\beta_{nd}^{\perp} + \beta_{df}^{\perp}}{\beta_{nd}^{\parallel} + \beta_{df}^{\parallel}}. \tag{13}$$

Analog to the step from Eqs. (6) to (7), now we obtain

$$\beta_{df} = \beta_{pf} \frac{(\delta_{pf} - \delta_{nd})(1 + \delta_{df})}{(\delta_{df} - \delta_{nd})(1 + \delta_{pf})} \quad \text{for } \delta_p > \delta_{nd}, \tag{14}$$

$$\beta_{df} = 0 \quad \text{for } \delta_p \leq \delta_{nd}. \tag{15}$$

which can be solved by assuming that the non-dust depolarization ratio is $\delta_{nd} = 0.05$ and the pure fine-mode dust depolarization ratio is $\delta_{df} = 0.16$ (see Fig. 5). Finally, we obtain the fine-mode backscatter coefficient for the remaining spherical particles,

$$\beta_{nd} = \beta_{pf} - \beta_{df}. \tag{16}$$

By using characteristic lidar ratios S_{df}, S_{dc}, and S_{nd} in Table 1 (for the Cyprus area in this study), we can convert the retrieved backscatter profiles β_{df}, β_{dc}, and β_{nd}, into respective particle extinction coefficient profiles for the three resolved aerosol components.

In the final step of the two-step POLIPHON retrieval, the set of particle backscatter and extinction coefficients are converted into particle volume and mass concentrations. The mass concentrations m_{df}, m_{dc}, and m_{nd} for fine dust, coarse dust, and non-dust particles, respectively, can be obtained from the backscatter coefficients β_{df}, β_{dc}, and β_{nd} by using the following relationships (Ansmann et al., 2011a, 2012):

$$m_{df} = \rho_d (v_{df}/\tau_{df}) \beta_{df} S_{df}\,, \tag{17}$$

$$m_{dc} = \rho_d (v_{dc}/\tau_{dc}) \beta_{dc} S_{dc}\,. \tag{18}$$

$$m_{nd} = \rho_{nd} (v_{nd}/\tau_{nd}) \beta_{nd} S_{nd}\,. \tag{19}$$

The particle densities ρ_d and ρ_{nd} are assumed to be 2.6 g m^{-3} and 1.5 g m^{-3}, respectively (Ansmann et al., 2012). The conversion factors v_m/τ_m with column particle volume concentration v_m and corresponding optical thickness τ_m for aerosol component m are obtained from photometer observations as shown in Sect. 3. An extended discussion on the range of observed conversion factors is given by Ansmann et al. (2012). As mentioned in Sect. 3, typical conversion factors are 0.6–0.9 × 10^{-6} m for supermicron dust, 0.25–0.4 × 10^{-6} m for submicron dust, and around 0.18 × 10^{-6} m for anthropogenic fine-mode aerosol.

4.2 Consistency check: POLIPHON vs. AERONET results

Because of the numerous assumptions and thus high degree of freedom in this two-step retrieval, we use AERONET observations as constraints to check the quality of the POLIPHON backscatter profiles. Goal is to check to what extend our results and the made assumptions are in consistency with the column values of aerosol optical properties as retrieved from accompanying sun/sky photometer observations.

The AERONET parameters useful for comparison are the aerosol particle optical thickness AOT_A, the Ångström exponent AE_A, and fine-mode fraction FMF_A. The respective lidar-derived quantities are AOT_L, AE_L, and FMF_L, which are calculated from the backscatter coefficient profiles in the planetary boundary layer (PBL) and the free troposphere (FT) and the parameters listed in Table 1. We distinguish local PBL aerosol particles and FT particles after long-range transport.

We define the lidar-derived optical depth for a given aerosol type m (nd: $m = 1$, df: $m = 2$, dc: $m = 3$) and layer l (planetary boundary layer, PBL: $l = 1$, free troposphere, FT: $l = 2$) as follows:

$$\tau_{m,l} = S_{m,l} \int_{z_{l,\text{bot}}}^{z_{l,\text{top}}} \beta_{m,l}(z)\,\mathrm{d}z\,. \tag{20}$$

Table 1 provides an overview of all input parameters. Lidar ratios for the PBL (lowest 300–450 m of the troposphere) are found around 30 sr because of the marine influence and around 60–80 sr in the FT from the CUT–AERONET long-term observations (2010–2014).

Because we compare in Sect. 4 solutions obtained with the one-step approach (nd: $m = 1$, d: $m = 2$ after Tesche et al., 2009) and the two-step method we introduce the parameter M with $M = 2$ in the case of the one-step method and $M = 3$ in the case of the two-step method. Now the total particle optical depth AOT_L derived from the lidar observations can be written as:

$$\tau_\text{L} = \sum_{m=1}^{M} \sum_{l=1}^{2} \tau_{m,l}\,. \tag{21}$$

The lidar-derived column Ångström exponent AE_L is given by

$$\alpha_\text{L} = \frac{\sum_{m=1}^{M} \sum_{l=1}^{2} \alpha_{m,l} \tau_{m,l}}{\sum_{m=1}^{M} \sum_{l=1}^{2} \tau_{m,l}} \tag{22}$$

with characteristic Ångström exponents in Table 1.

Typical Ångström exponents in Table 1 for the free troposphere and boundary-layer aerosol over Cyprus are obtained from the long-term AERONET–EARLINET studies (2010–2014). The pure dust Ångström exponents are from the SAMUM-1 campaign.

The fine-mode fraction FMF_L is computed from the lidar data as follows:

$$f_L = \frac{\sum_{m=1}^{M-1} \sum_{l=1}^{2} \tau_{m,l}}{\sum_{m=1}^{M} \sum_{l=1}^{2} \tau_{m,l}}. \quad (23)$$

4.3 Retieval uncertainties

Uncertainties in the separation of the backscatter coefficients of spherical particles and fine and coarse dust particles are caused by four sources: (a) uncertainties in the computation of the basic products, i.e., of the particle depolarization ratios and backscatter coefficients, (b) uncertainties in the assumptions on characteristic depolarization ratios for fine dust and coarse dust, (c) uncertainties in the assumption of the contribution of haze and smoke particles to the free tropospheric aerosol, and (d) uncertainties in the input parameters in Table 1. According to the error discussions by Tesche et al. (2009) and Mamouri et al. (2013) the overall uncertainty in the separation of the backscatter coefficients for the different aerosol types is of the order 20–40 %. The uncertainty in the retrieved mass concentration profiles may be of the order of 50 %. However, as the good agreement and consistency between the lidar and AERONET photometer observations in the next section indicate, the retrieval uncertainties are usually much lower (of the order of 25 % or even less). In this first feasibility study on the potential of polarization lidar to provide detailed insight into fine-mode and coarse-mode dust optical and microphysical properties we avoid to present error bars in the next section to keep the figures simple and to facilitate the discussion.

Another error source arises from a potential interference by other non-spherical aerosol types. The lidar/photometer data analysis and interpretation must be always accompanied by extended backward trajectory analysis and atmospheric transport model simulations to be sure that soil or desert dust is the only aerosol component that significantly depolarises backscattered laser light. In 2010, volcanic dust emitted by the Islandic volcano Eyjafjallajökull and Saharan dust occured simultaneously over wide areas of southeastern Europe and complicated the aerosol lidar data analysis

AMTD
7, 5173–5221, 2014

(Papayannis et al., 2012). Also, dried marine particles, e.g., sea salt particles after advection over land at relative humidities below 50–70 %, may disturb the polarization observations at lidar sites on islands and coastal areas. Sakai et al. (2010) demonstrated that dry, irregularly shaped sea salt particles can cause a depolarization ratio of 9 % (fine-mode). One can conclude from studies of Murayama et al. (1999) that dry coarse sea salt aerosol may lead to particle depolarization ratios of 20–25 %. However, the long-term observations at Cyprus indicate that marine particles are usually spherical and show low depolarization ratios < 3 % as typical for marine environments (Groß et al., 2011). In addition, marine particles are widely confined to the lowermost 500–800 m (marine boundary layer) of the atmosphere and have a minor impact on free tropospheric aerosol properties.

5 Results: 26–30 September 2011 case study

5.1 Overview

The following case study serves as a testbed for the applicability of the new two-step POLIPHON method. Both, the one-step and the two-step method are used to analyse a period with background fine soil dust and desert dust from Syria. Layers of soil dust particles are frequently advected to Cyprus from areas of central and eastern Turkey and other arid regions further north of Turkey during the summer season. These layers occur as lofted, vertically homogeneous plumes mostly in the height range of 1–3 km a.s.l. As a unique feature, this background soil dust mainly consists of submicron particles as the AE_A values indicate. A coarse-mode fraction is not or almost not visible in the photometer observations. The reason for the absence of coarse dust particles is not clear. Particle sedimentation, removal of predominately large particles by cloud processes and washout effects, and depletion of the source region with respect to coarse material may have contributed to the observed low amount of coarse dust particles. Episodically desert dust outbreaks with a pronounced number concentration of

Discussion Paper | Discussion Paper | Discussion Paper | Discussion Paper |
AMTD
7, 5173–5221, 2014
Fine and coarse dust profiling
R. E. Mamouri and A. Ansmann

supermicron particles from deserts in the Middle East and northern Africa reach Limassol and partly mix with this fine-mode soil dust from the north. One of such events is discussed in this section.

Figure 6 shows the arrival of an extended desert dust layer over Limassol in the late morning of 28 September 2011. Before, a northerly airflow from Turkey prevailed according to the backward trajectories in Fig. 7. The air mass transport changed from northerly advection on 26–27 September 2011 to more complex features in the regional aerosol transport resulting from a major Arabian dust outbreak on 28–29 September 2011.

The particle size distributions in Fig. 8 (taken from the AERONET data base, level 2.0 data) show a bimodal shape with a strong increase of the coarse-mode fraction when the dust outbreak arrived. The weak coarse mode on 26–27 September 2011 (blue lines in Fig. 8) consists most likely of marine particles as Fig. 9 suggests. In this figure, pure marine size distributions as observed over Barbados with AERONET photometers during a field campaign (see AERONET site of Barbados–SALTRACE, located at the west coast of Barbados, at the Caribbean Institute for Meteorology and Hydrology, CIMH) and at Ragged Point (east coast of Barbados) are compared with the observations over Limassol on 26–27 September 2011. As can be seen, the coarse modes over Limassol and Barbados are rather similar. Thus the marine aerosol impact may fully explain the occurrence of the coarse mode in the volume size distributions of the Cyprus AERONET site on 26–27 September 2011. Marine particles are confined to heights of 300–450 m during the period studied here.

Typical marine AOTs are of the order of 0.04–0.06 at 500 nm with a fine-mode contribution of 40–50 % as can be seen in Fig. 9 for the Barbados cases. If we subtract a potential fine-mode marine contribution of 0.025–0.03 and a similar urban-haze contribution from the observed fine-mode AOT of 0.172, about 0.1–0.12 is left for the fine-mode aerosol in the free troposphere on 26–27 September 2011. The depolarization ratio profile in Fig. 10 shows that this fine-mode aerosol produces significantly enhanced depolarization ratios around 10–15 %. A considerable fraction of the free tropospheric fine-mode aerosol must therefore be dust. Since the aerosol crosses populated and industrialized areas in Turkey and further to the north, we must assume that a mixture of fine dust and other (spherical) aerosol components (urban haze, fire smoke) was present and lowered the overall particle depolarization ratio. As can be seen in Fig. 10, the depolarization ratio went up to almost 0.35 on 28 September 2011, when the Arabian dust arrived.

An overview of the AERONET photometer observations from 26–30 September is presented in Fig. 11. The 500 nm AOT_A increased to values around 0.7 during the desert dust outbreak in the morning of 29 September 2011. At the same time, the 500 nm FMF_A droped to values of 0.25. During the fine-mode dust days (26–27 September), FMF_A was high with values > 0.9. Later on the values from 0.4 and 0.7 indicated mixed aerosols. The Ångström exponent AE_A was around 1.8 during the fine-mode dust days and dropped to values of 0.5–1.0 when the major dust outbreak dominated the aerosol conditions over Limassol. The minimum value of $AE_A = 0.25$ was observed in the early morning of 29 September 2011.

5.2 Retrieval of fine-mode and coarse-mode backscatter coefficients

Figures 12–15 show examples of applications of the new two-step method in terms of the basic quantities, the backscatter coefficients. For comparison, the particle backscatter coefficients obtained with the one-step method are shown in the central panels of these figures, assuming typical depolarization ratios of 0.05 and 0.31 for dust and non-dust particles (see Fig. 5). In the case of the two-step method, the characteristic particle depolarization ratios are 0.05, 0.16, and 0.39 for spherical particles, fine dust, and coarse dust, respectively, As outlined in Sect. 4, it is assumed that roughly 25 % of the fine particles in the free troposphere are of anthropogenic origin (urban haze and biomass burning smoke).

The aerosol conditions as observed before the arrival of the major dust storm are given in Fig. 12. The free tropospheric aerosol layer extended from about 350 to 3500 m height. The particle depolarization ratio range from 0.1–0.14 in the main aerosol layer

AMTD
7, 5173–5221, 2014

R. E. Mamouri and A. Ansmann

up to 2500 m. The slightly enhanced depolarization ratio values in the boundary layer (< 300 m) are probably caused by road dust and surface-near local dust transport from arid regions of Cyprus. The colored numbers in Fig. 12 are the lidar-derived AOT_L values (after Eq. 20) for the different aerosol components. In addition, the lidar-derived Ångström exponent AE_L (Eq. 22) and fine-mode fraction FMF_L (Eq. 23) are presented and compared with respective AERONET values (FMF_A, AE_A) given in the left panels of the figures.

As can be seen in Fig. 12, the one-step method leads to a comparably large coarse-mode particle backscatter fraction for depolarization ratios of 0.1–0.14. Accordingly, FMF_L is much lower with 0.71 at these specific background fine-mode dust conditions than the AERONET value of $FMF_A = 0.92$. As a consequence, a significant disagreement is also found in terms of the Ångström exponent ($AE_A = 1.68$, $AE_L = 1.42$). A much better agreement is obtained when using the two-step method. The fine-mode fraction now consists of spherical particles and fine-mode dust. This leads to an increase in FMF_L and AE_L values.

Figure 13 shows the aerosol conditions after the arrival of desert dust. A pronounced dust layer was found between 1 and 2 km height, and high depolarization ratios of > 0.3 were observed in this layer indicating a strong contribution of coarse dust particles to light backscattering (see Fig. 10). The AERONET values of AE_A and FMF_A significantly decreased compared to the values observed the day before (Fig. 11). Both, the application of the one-step and the two-step method, reveal large coarse-dust-related backscatter coefficients between 1 and 2 km height and a mixture of fine-mode and coarse-mode particles below and above the main desert dust layer. As can be seen in the right panels of Fig. 13, a considerable part of the fine-mode backscatter coefficient is caused by dust. By resolving fine and coarse dust again a better agreement of the AERONET and lidar-derived AE and FMF values is obtained.

Figure 14 provides more insight into the two-step data analysis (same case as in Fig. 13, top panels). By using the depolarization limits of 0.12 and 0.39 we determine the contributions of fine-mode particles and coarse dust particles (see Fig. 5, first step

AMTD
7, 5173–5221, 2014

of the two-step method). Before we can apply the second step we have to remove the coarse dust impact on the backscatter coefficient by means of Eq. (9) and on the particle depolarization ratio by means of Eq. (10) or Eqs. (11) and (12). These resulting coarse-dust-corrected backscatter and depolarization ratio profiles are shown in Fig. 14 as blue dashed lines. They are the input profiles for the second round of the two-step method to reveal the backscatter coefficient profiles for fine-mode spherical particles and fine-mode dust. Since we assumed a fixed ratio of fine spherical particles and fine dust ratio (assuming about 75 % fine dust in the fine mode) in the two-step data analysis, the ratio of obtained particle backscatter coefficients for fine spherical particle to fine dust may give a rough hint how justified this assumption is. As shown in the figure, the ratio of the blue and orange backscatter profiles is about 0.5–0.66 throughout the lowest 2 km of the troposphere which is close the assumed value of around 0.75.

Figure 15 shows the situation of 29 September 2011 when the desert dust plume influenced the entire tropospheric column up to 2.5 km height and covered large parts of the eastern Mediterranean. The 500 nm AOT was close to 0.43 with a strong coarse dust contribution of 0.235 (two-step method). Both, the one-step and the two-step method, reveal a total dust AOT close to 0.35. Again the two-step method results (AE_L, FMF_L) are in better agreement with the AERONET products (AE_A, FMF_A) than the values obtained with the one-step approach. The one-step method yields a rather low fine-mode fraction of 0.19 which is similar to the spherical mode fraction of $SMF_L = 0.18$ in the case of the two-step method.

5.3 Consistency check with AERONET results

Figures 16 and 17 provide an overview of the AERONET and lidar-derived AE and FMF values for the entire observational period from 26–30 September 2011. The AE_L values depend on many assumptions regarding the spectral dependence of backscattering and extinction of a variety of aerosol types (according to Table 1). Therefore, the comparison with the AE_A values may only provide hints on the quality of the AE_L values. The FMF values, on the other hand, are not largely influenced by assumptions

AMTD
7, 5173–5221, 2014

R. E. Mamouri and A. Ansmann

so that the good agreement with FMF_A is a clear sign that our two-step approach worked successful. Especially for 26–29 September period a very good agreement of the AERONET and the two-step-method results is obtained. At the end of our observational period (30 September 2011), when the backward trajectories (not presented) showed a complex air mass transport structure with prevailing westerly winds, both methods are no longer in good agreement with the AERONET results because of the undefined conditions on mixing of marine, urban smoke, and dust aerosols.

5.4 Particle extinction and mass concentration profiles

Finally, Fig. 18 provides an example for the computation of the particle extinction coefficients and mass concentrations from the particle backscatter coefficients. These retrievals complete the POLIPHON data analysis. For each aerosol component (fine spherical, fine dust, coarse dust), extinction and mass profiles are presented. The results for the lowermost 300 m have to be interpreted with caution because all profiles rely on the assumption of a linear increase of the backscatter coefficient from 300 m towards the ground.

As can be seen in Fig. 18, fine-mode dust significantly contributes to the total particle extinction coefficient in the free troposphere as demonstrated in Sect. 3. Extinction values for fine-mode dust are of the order of 30–50 Mm^{-1}.

The mass concentration profiles show that coarse dust mostly contributes to particle mass in the free troposphere. Maximum values of close to 1000 $\mu g\,m^{-3}$ are found at 1.2 km height. Fine dust mass concentrations are around 40 $\mu g\,m^{-3}$ in the free troposphere and 50–100 $\mu g\,m^{-3}$ close to the ground. The fine sphercial particles show much less mass concentrations of 15–20 $\mu g\,m^{-3}$ in the PBL and 10–15 $\mu g\,m^{-3}$ in the free troposphere. Thus, fine dust can dominate $PM_{1.0}$ levels at ground during dust outbreak situations.

AMTD
7, 5173–5221, 2014

R. E. Mamouri and A. Ansmann

6 Conclusions

The separation of profiles of fine dust and coarse dust optical properties by means of the polarization lidar technique has been proposed for the first time. The presented new lidar method is an extension of the traditional method applied to distinguish non-sphercial and spherical particles. Now, fine-mode and coarse-mode dust profiles in terms of particle backscatter and extinction coefficients, volume and mass concentratiosn can be derived. A feasibility study based on complex aerosol observations with EARLINET lidar and AERONET sun/sky photometer observations over Limassol, Cyprus, demonstrated the applicability and usefulness of the new two-step POLIPHON method. Good agreement with AERONET column aerosol observations was found. Such a step forward in the application of polarization lidar technique provides important new insight into dust properties for atmospheric and environmental research.

It should be emphasized that the developed one-wavelength polarization method as presented here is only one of several potential ways to retrieve fine and coarse-mode dust profiles. The new retrieval technique requires a considerably number of assumptions. Nevertheless, the advantage of simple lidars is that they are usually robust and favorable for long-term monitoring efforts.

In the next step, multiwavelength polarization lidars, providing depolarization ratios at two wavelengths (Sugimoto and Lee, 2006; Groß et al., 2011; Kanitz et al., 2014) or even three wavelengths (Ansmann et al., 2014; Müller et al., 2014), with additional Raman or high-spectral-resolution channels for extinction and backscattering profiling, are best candidates for an almost unambiguous separation of fine and coarse dust profiles. Based on the measured wavelength dependence of light depolarization, backscattering and extinction coefficients, three to four aerosol types (marine, haze and smoke, fine dust, coarse dust) which all have different characteritsics in terms of particle depolarization ratio and wavelength dependence of backscattering and extinction, can then be discriminated.

It should also be mentioned that the LIRIC and GARRLiC methods are able to separate fine-mode and coarse-mode dust. According to the theoretical backround these methods distinguish fine-mode spherical, fine-mode non-spherical, coarse-mode spherical, and coarse-mode non-spherical particle types. Also the technique presented by David et al. (2013) is capable to provide separate information on fine and coarse dust profiles. However, these techniques are all based on a particle shape models (assuming dust particles to be spheroids). This assumption causes considerable uncertainties.

As a final remark we would like to emphasis that further laboratory studies (for the laser wavelength of 355, 532, and 1064 nm) and efforts of modelling of the dust optical properties such as the particle depolarization ratio and lidar ratio, separately for irregularly shaped fine dust and coarse dust are required. We used the best available information for our separation method, but studies explicitely focussing on the depolarizing effects of realistic fine mode and coarse dust ensembles are not available.

Acknowledgements. The authors thank the CUT Remote Sensing Laboratory for their support. We are grateful to AERONET for high-quality sun/sky photometer measurements in Cyprus, Morocco, and Barbados. The authors gratefully acknowledge the NOAA Air Resources Laboratory (ARL) for the provision of the HYSPLIT transport and dispersion model and/or READY website (http://www.ready.noaa.gov) used in this publication.

References

Ångström, A.: The parameters of atmospheric turbidity, Tellus, 16, 64–75, 1964. 5179

Ansmann, A., Bösenberg, J., Chaikovsky, A., Comerón, A., Eckhardt, S., Eixmann, R., Freudenthaler, V., Ginoux, P., Komguem, L., Linné, H., López Márquez, M. A., Matthias, V., Mattis, I., Mitev, V., Müller, D., Music, S., Nickovic, S., Pelon, J., Sauvage, L., Sobolewsky, P., Srivastava, M. K., Stohl, A., Torres, O., Vaughan, G., Wandinger, U., and Wiegner, M.: Long-range transport of Saharan dust to northern Europe: the 11–16 October 2001 outbreak observed with EARLINET, J. Geophys. Res., 108, 4783, doi:10.1029/2003JD003757, 2003. 5174

Ansmann, A., Tesche, M., Seifert P, Groß, S., Freudenthaler, V., Apituley, A., Wilson, K. M., Serikov, I., Linné, H., Heinold, B., Hiebsch, A., Schnell, F., Schmidt, J., Mattis, I., Wandinger, U., and Wiegner, M.: Ash and fine-mode particle mass profiles from EARLINET-AERONET observations over central Europe after the eruptions of the Eyjafjallajökull volcano in 2010, J. Geophys. Res., 116, D00U02, doi:10.1029/2010JD015567, 2011a. 5175, 5186

Ansmann, A., Petzold, A., Kandler, K., Tegen, I., Wendisch, M., Müller, D., Weinzierl, B., Müller, T., and Heintzenberg, J.: Saharan mineral dust experiments SAMUM-1 and SAMUM-2: What have we learned?, Tellus B, 63, 403–429, doi:10.1111/j.1600-0889.2011.00555.x, 2011b. 5180

Ansmann, A., Seifert, P., Tesche, M., and Wandinger, U.: Profiling of fine and coarse particle mass: case studies of Saharan dust and Eyjafjallajökull/Grimsvötn volcanic plumes, Atmos. Chem. Phys., 12, 9399–9415, doi:10.5194/acp-12-9399-2012, 2012. 5175, 5176, 5186

Ansmann, A., Althausen, D., Kanitz, T., Engelmann, R. Skupin, A., Baars, H., Klepel, A., Haarig, M., Heinold, B., Tegen, I., Toledano, C., Prescod, D., and Farrell, D., Saharan dust long-range transport: SALTRACE lidar observations at Barbados and aboard RV Meteor (Guadeloupe to Cape Verde) versus dust transport modelling, Proceedings, DUST 2014 – International Conference on Atmospheric Dust, Castellaneta Marina, Italy, 1–6 June 2014, 2014. 5195

Baars, H., Ansmann, A., Althausen, D., Engelmann, R., Artaxo, P., Pauliquevis, T., and Souza, R.: Further evidence for significant smoke transport from Africa to Amazonia, Geophys. Res. Lett., 38, L20802, doi:10.1029/2011GL049200, 2011. 5174

Barnaba, F. and Gobbi, G. P.: Aerosol seasonal variability over the Mediterranean region and relative impact of maritime, continental and Saharan dust particles over the basin from MODIS data in the year 2001, Atmos. Chem. Phys., 4, 2367–2391, doi:10.5194/acp-4-2367-2004, 2004. 5181

Burton, S. P., Vaughan, M. A., Ferrare, R. A., and Hostetler, C. A.: Separating mixtures of aerosol types in airborne High Spectral Resolution Lidar data, Atmos. Meas. Tech., 7, 419–436, doi:10.5194/amt-7-419-2014, 2014. 5177

Chaikovsky, A., Dubovik, O., Goloub, P., Tanré, D., Pappalardo, G., Wandinger, U., Chaikovskaja, L., Denisov, S., Grudo, Y., Lopatsin, A., Karol, Y., Lapyonok, T., Korol, M., Osipenko, F., Savitsky, D., Slesar, A., Apituley, A., Alados-Arboledas, L., Binietoglou, I., Comerón, A., Granados–Muñoz, M. J., Papayanis, A., Perrone, M. R., Pietruczuk, A., De Tomasi, F., Wagner, J., and Wang, X.: Algorithm and software for the retrieval of vertical

AMTD
7, 5173–5221, 2014

Fine and coarse dust profiling

R. E. Mamouri and A. Ansmann

aerosol properties using combined lidar/radiometer data: dissemination in EARLINET network, Proceedings, 26th International Laser Radar Conference, Porto Heli, Greece, 399–402, 2012. 5176

Chen, W.-N., Tsai, F.-J., Chou, C. C.-K., Chang, S.-Y., Chen, Y.-W., and Chen, J.-P.: Optical properties of Asian dusts in the free atmosphere measured by Raman lidar at Taipei, Taiwan, Atmos. Environ., 41, 7698–7714, 2007. 5182

DeMott, P. J., Prenni, A. J., Liu, X., Kreidenweis, S. M., Petters, M. D., Twohy, C. H., Richardson, M. S., Eidhammer, T., and Rogers, D. C.: Predicting global atmospheric ice nuclei distributions and their impacts on climate, P. Natl. Acad. Sci. USA, 107, 11217–11222, doi:10.1073/pnas.0910818107, 2010. 5175

David, G., Thomas, B., Nousiainen, T., Miffre, A., and Rairoux, P.: Retrieving simulated volcanic, desert dust and sea-salt particle properties from two/three-component particle mixtures using UV-VIS polarization lidar and T matrix, Atmos. Chem. Phys., 13, 6757–6776, doi:10.5194/acp-13-6757-2013, 2013. 5196

Dubovik, O., Sinyuk, A., Lapyonok, T., Holben, B., Mishchenko, M., Yang, P., Eck, T., Volten, H., Muñoz, O., Veihelmann, B., van der Zande, W. J., Leon, J. F., Sorokin, M., and Slutsker, I.: Application of spheroid models to account for aerosol particle non-sphericity in remote sensing of desert dust, J. Geophys. Res., 111, D11208, doi:10.1029/2005JD006619, 2006. 5177

Fiebig, M., Petzold, A., Wandinger, U., Wendisch, W., Kiemle, C., Stifter, A., Ebert, M., Rother, T., and Leiterer, U.: Method, accuracy, and inferable properties applied to a biomass-burning aerosol and its radiative forcing, J. Geophys. Res., 107, 8130, doi:10.1029/2000JD000192, 2002. 5182

Freudenthaler, V., Esselborn, M., Wiegner, M., Heese, B., Tesche, M., Ansmann, A., Müller, D., Althausen, D., Wirth, M., Fix, A., Ehret, G., Knippertz, P., Toledano, C., Gasteiger, J., Garhammer, M., and Seefeldner, M.: Depolarization ratio profiling at several wavelengths in pure Saharan dust during SAMUM 2006, Tellus B, 61, 165–179, doi:10.1111/j.1600-0889.2008.00396.x, 2009. 5176, 5178, 5179, 5182, 5203

Gasteiger, J., Wiegner, M., Groß, S., Freudenthaler, V., Toledano, C., Tesche, M., and Kandler, K.: Modelling lidar-relevant optical properties of complex mineral dust aerosols, Tellus B, 63, 725–741, doi:10.1111/j.1600-0889.2011.00559.x, 2011. 5176

Groß, S., Tesche, M., Freudenthaler, V., Toledano, C., Wiegner, M., Ansmann, A., Althausen, D., and Seefeldner, M.: Characterization of Saharan dust, marine aerosols and mixtures of biomass-burning aerosols and dust by means of multi-wavelength depolarization and Ra-

Discussion Paper | Discussion Paper | Discussion Paper | Discussion Paper |

man lidar measurements during SAMUM 2, Tellus B, 63, 706–724, doi:10.1111/j.1600-0889.2011.00556.x, 2011. 5175, 5176, 5182, 5189, 5195, 5203

Groß, S., Esselborn, M., Weinzierl, B., Wirth, M., Fix, A., and Petzold, A.: Aerosol classification by airborne high spectral resolution lidar observations, Atmos. Chem. Phys., 13, 2487–2505, doi:10.5194/acp-13-2487-2013, 2013. 5177

Heese, B. and Wiegner, M.: Vertical aerosol profiles from Raman polarization lidar observations during the dry season AMMA field campaign, J. Geophys. Res., 113, D00C11, doi:10.1029/2007JD009487, 2008. 5182

Heintzenberg, J.: The SAMUM-1 experiment over Southern Morocco: overview and introduction, Tellus B, 61, 2–11, 2009. 5180

Holben, B. N., Eck, T. F., Slutsker, I., Tanré, D., Buis, J. P., Setzer, A., Vermote, E., Reagan, J. A., Kaufman, Y. J., Nakajima, T., Lavenu, F., Jankowiak, I., and Smirnov, A.: AERONET – a federated instrument network and data archive for aerosol characterization, Remote Sens. Environ., 66, 1–16, 1998. 5179

Kanitz, T., Engelmann, R., Heinold, B., Baars, H., Skupin, A., and Ansmann, A.: Tracking the Saharan air layer with shipborne lidar across the tropical Atlantic, Geophys. Res. Lett., 41, 4762–4766, doi:10.1002/2013GL058780, 2014. 5195

Kok, J. F.: A scaling theory for the size distribution of emitted dust aerosols suggests climate models underestimate the size of the global dust cycle, P. Natl. Acad. Sci. USA, 108, 1016–1021, doi:10.1073/pnas.1014798108, 2011. 5175

Lopatin, A., Dubovik, O., Chaikovsky, A., Goloub, P., Lapyonok, T., Tanré, D., and Litvinov, P.: Enhancement of aerosol characterization using synergy of lidar and sun-photometer coincident observations: the GARRLiC algorithm, Atmos. Meas. Tech., 6, 2065–2088, doi:10.5194/amt-6-2065-2013, 2013. 5176

Mahowald, N., Albani, S., Kok, J. F., Engelstaeder, S., Scanza, R., Ward, D. S., and Flanner, M. G.: The size distribution of desert dust aerosols and its impact on the Earth system, Aeolin Research, online first, doi:10.1016/j.aeolia.2013.09.002, 2014. 5175

Mamouri, R. E., Ansmann, A., Nasantzi, A., Kokkalis, P., Schwarz, A., and Hadjimitsis, D.: Low Arabian extinction-to-backscatter ratio, Geophys. Res. Lett., 40, 4762–4766, doi:10.1002/grl.50898, 2013. 5178, 5179, 5188, 5203, 5213

Murayama, T., Okamoto, H., Kaneyasu, N., Kamataki, H., and Miura, K.: Application of lidar depolarization measurement in the atmospheric boundary layer: effects of dust and sea-salt particles, J. Geophys. Res., 104, 31781–31792, doi:10.1029/1999JD900503, 1999. 5182, 5189

Murayama, T., Müller, D., Wada, K., Shimizu, A., Sekiguchi, M., and Tsukamoto, T.: Characterization of Asian dust and Siberian smoke with multiwavelength Raman lidar over Tokyo, Japan in spring 2003, Geophys. Res. Lett., 31, L23103, doi:10.1029/2004GL021105, 2004. 5182

Müller, D., Mattis, I., Wandinger, U., Ansmann, A., Althausen, A., and Stohl, A.: Raman lidar observations of aged Siberian and Canadian forest fire smoke in the free troposphere over Germany in 2003: microphysical particle characterization, J. Geophys. Res., 110, D17201, doi:10.1029/2004JD005756, 2005. 5182

Müller, D., Ansmann, A., Mattis, I., Tesche, M., Wandinger, U., Althausen, D., and Pisani, G.: Aerosol-type-dependent lidar ratios observed with Raman lidar, J. Geophys. Res., 112, D16202, doi:10.1029/2006JD008292, 2007. 5182, 5203

Müller, D., Hostetler, C. A., Ferrare, R. A., Burton, S. P., Chemyakin, E., Kolgotin, A., Hair, J. W., Cook, A. L., Harper, D. B., Rogers, R. R., Hare, R. W., Cleckner, C. S., Obland, M. D., Tomlinson, J., Berg, L. K., and Schmid, B.: Airborne multiwavelength High Spectral Resolution Lidar (HSRL-2) observations during TCAP 2012: vertical profiles of optical and microphysical properties of a smoke/urban haze plume over the northeastern coast of the US, Atmos. Meas. Tech. Discuss., 7, 1059–1073, doi:10.5194/amtd-7-1059-2014, 2014. 5195

Nabat, P., Solmon, F., Mallet, M., Kok, J. F., and Somot, S.: Dust emission size distribution impact on aerosol budget and radiative forcing over the Mediterranean region: a regional climate model approach, Atmos. Chem. Phys., 12, 10545–10567, doi:10.5194/acp-12-10545-2012, 2012. 5175

Nishizawa, T., Okamoto, H., Sugimoto, N., Matsui, I., Shimizu, A., and Aoki, K.: An algorithm that retrieves aerosol properties from dual-wavelength polarized lidar measurements, J. Geophys. Res., 112, D06212, doi:10.1029/2006JD007435, 2007. 5175

O'Neill, N. T., Eck, T. F., Smirnov, A., Holben, B. N., and Thulasiraman, S.: Spectral discrimination of coarse and fine mode optical depth, J. Geophys. Res., 108, 4559, doi:10.1029/2002JD002975, 2003. 5179

Papayannis, A., Amiridis, V., Mona, L., Tsaknakis, G., Balis, D., Bösenberg, J., Chaikovski, A., De Tomasi, F., Grigorov, I., Mattis, I., Mitev, V., Müller, D., Nickovic, S., Pérez, C., Pietruczuk, A., Pisani, G., Ravetta, F., Rizi, V., Sicard, M., Trickl, T., Wiegner, M., Gerding, M., Mamouri, R. E., D'Amico, G., and Pappalardo, G.: Systematic lidar observations of Saharan

AMTD
7, 5173–5221, 2014

Fine and coarse dust profiling

R. E. Mamouri and A. Ansmann

dust over Europe in the frame of EARLINET (2000–2002), J. Geophys. Res., 113, D10204, doi:10.1029/2007JD009028, 2008. 5174

Papayannis, A., Mamouri, R. E., Amiridis, V., Giannakaki, E., Veselovskii, I., Kokkalis, P., Tsaknakis, G., Balis, D., Kristiansen, N. I., Stohl, A., Korenskiy, M., Allakhverdiev, K., Huseyinoglu, M. F., and Baykara, T.: Optical properties and vertical extension of aged ash layers over the Eastern Mediterranean as observed by Raman lidars during the Eyjafjallajökull eruption in May 2010, Atmos. Environ., 48, 56–65, 2012 5189

Sakai, T., Nagai, T., Zaizen, Y, and Mano, Y.: Backscattering linear depolarization ratio measurements of mineral, sea-salt, and ammonium sulfate particles simulated in a laboratory chamber, Appl. Optics, 49, 4441–4449, 2010. 5175, 5176, 5183, 5185, 5189, 5203

Sasano, Y., Browell, E. V., and Ismail, S.: Error caused by using a constant extinction/backscattering ratio in the lidar solution, Appl. Optics, 24, 3929–3932, 1985. 5179

Shimizu, A., Sugimoto, N., Matsui, I., Arao, K., Uno, I., Murayama, T., Kagawa, N., Aoki, K., Uchiyama, A., and Yamazaki, A.: Continuous observations of Asian dust and other aerosols by polarization lidars in China and Japan during ACE-Asia, J. Geophys. Res., 109, D19S17, doi:10.1029/2002JD003253, 2004. 5182

Sugimoto, N. and Lee, C. H.: Characteristics of dust aerosols inferred from lidar depolarization measurements at two wavelength, Appl. Optics, 45, 7468–7474, 2006 5175, 5182, 5195

Sugimoto, N., Uno, I., Nishikawa, M., Shimizu, A., Matsui, I., Dong, X., Chen, Y., and Quan, H.: Record heavy Asian dust in Beijing in 2002: Observations and model analysis of recent events, Geophys. Res. Lett., 30, 1640, doi:10.1029/2002GL016349, 2003. 5182

Tesche, M., Ansmann, A., Müller, D., Althausen, D., Engelmann, R., Freudenthaler, V., and Groß, S.: Vertically resolved separation of dust and smoke over Cape Verde using multiwavelength Raman and polarization lidars during Saharan Mineral Dust Experiment 2008, J. Geophys. Res., 114, D13202, doi:10.1029/2009JD011862, 2009. 5175, 5181, 5188

Tesche, M., Müller, D., Groß, S., Ansmann, A., Althausen, D., Freudenthaler, V., Weinzierl, B., Veira, A., and Petzold, A.: Optical and microphysical properties of smoke over Cape Verde inferred from multiwavelength lidar measurements, Tellus B, 63, 677–694, doi:10.1111/j.1600-0889.2011.00549.x, 2011. 5175

Wandinger, U. and Ansmann, A.: Experimental determination of the lidar overlap profile with Raman lidar, Appl. Optics, 41, 511–514, 2002. 5178

Wagner, J., Ansmann, A., Wandinger, U., Seifert, P., Schwarz, A., Tesche, M., Chaikovsky, A., and Dubovik, O.: Evaluation of the Lidar/Radiometer Inversion Code (LIRIC) to determine microphysical properties of volcanic and desert dust, Atmos. Meas. Tech., 6, 1707–1724, doi:10.5194/amt-6-1707-2013, 2013. 5177

Zhang, L., Kok, J. F., Henze, D. K., Li, Q., and Zhao, C.: Improving simulations of fine dust surface concentrations over the western United States by optimizing the particle size distribution, Geophys. Res. Lett., 40, 3270–3275, doi:10.1002/grl.50591, 2013. 5175

AMTD

7, 5173–5221, 2014

Table 1. Overview of all input parameters used in our study. The particle lidar ratios and the PBL and FT Ångström exponents for non-dust aerosol are based on a careful analysis of the AERONET data in combination with the EARLINET data set for 2010–2014 with and without lofted aerosol layers in the FT over Limassol. SAMUM-1 observations provided the dust Ångström exponents. The depolarization ratios are taken from the literature. The indices nd, df, dc, d as used in the retrieval in Sect. 4 denote non-spherical particles, fine-mode dust, coarse-mode dust, and total (fine and coarse) dust, respectively.

Parameter	Symbol	Value	Source/reference
Particle lidar ratio (marine)		20 sr	Groß et al. (2011)
Particle lidar ratio (dust)	S_{df}, S_{dc}	35–40 sr	Mamouri et al. (2013)
Particle lidar ratio (urban haze, smoke)		50–70 sr	CUT, climatology
Particle lidar ratio (PBL, spherical)	S_{nd}(PBL)	30 sr	CUT, climatology
Particle lidar ratio (FT, spherical)	S_{nd}(FT)	60–80 sr	CUT, climatology
Ångström Exponent (PBL, spherical)	α_{nd}(PBL)	0.5–1.5	CUT, climatology
Ångström Exponent (FT, spherical)	α_{nd}(FT)	2.0	CUT, climatology
Ångström Exponent (fine dust)	α_{df}	1.5	SAMUM-1, Fig. 3
Ångström Exponent (coarse dust)	α_{dc}	−0.2	SAMUM-1, Fig. 3
Ångström Exponent (total dust)	α_{d}	0.25	SAMUM-1, Fig. 3
Particle linear depolarization ratio (spherical)	δ_{nd}	0.05	Müller et al. (2007)
Particle linear depolarization ratio (fine dust)	δ_{df}	0.16	Sakai et al. (2010)
Particle linear depolarization ratio (coarse dust)	δ_{dc}	0.39	Sakai et al. (2010)
Particle linear depolarization ratio (total dust)	δ_{d}	0.31	Freudenthaler et al. (2009)

AMTD
7, 5173–5221, 2014

R. E. Mamouri and A. Ansmann

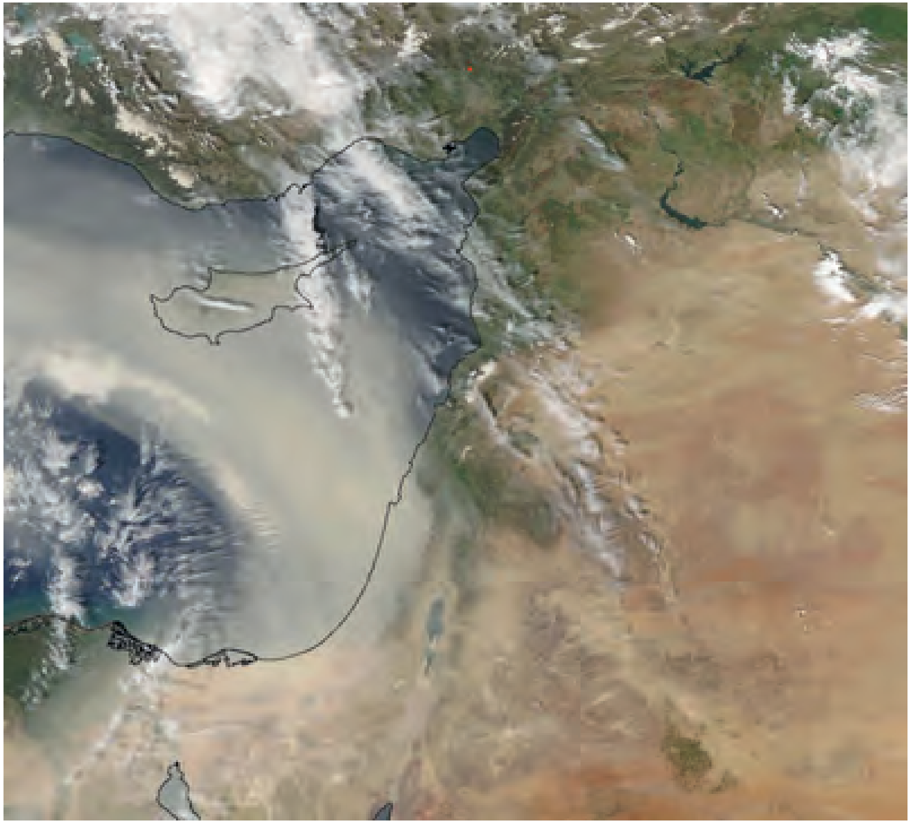

Figure 1. Major Saharan dust outbreak moving northward and striking Cyprus on 1 April 2013 (AQUA-MODIS image, 10:40 UTC).

AMTD

7, 5173–5221, 2014

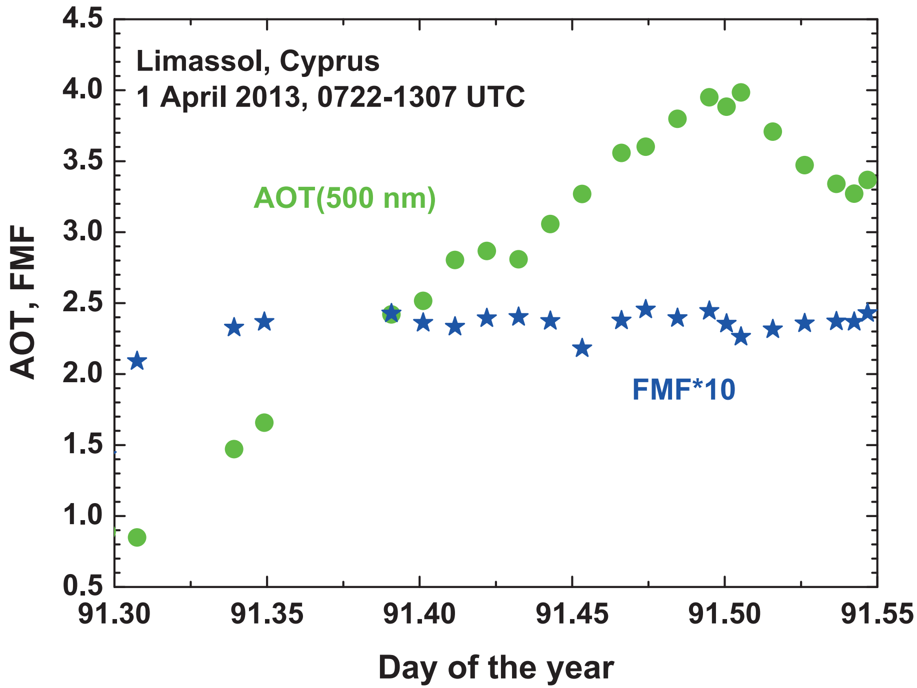

Figure 2. 500 nm aerosol particle optical thickness (AOT, green circles) and fine-mode fraction (FMF multiplied by a factor of 10, blue stars), observed with AERONET sun/sky photometer on 1 April 2013. Peak AOT values reached 4.0 around noon. The dust-dominated FMF was always close to 0.24.

AMTD
7, 5173–5221, 2014

R. E. Mamouri and A. Ansmann

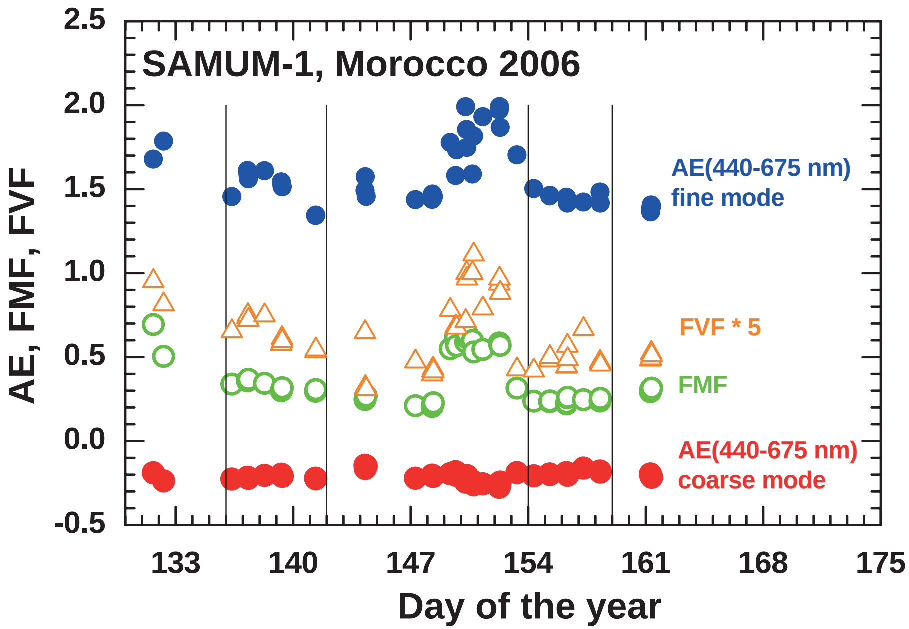

Figure 3. SAMUM-1 pure Saharan dust Ångström exponent AE (440–675 wavelength range) for fine mode (blue circles) and coarse mode (red circles), fine-mode 500 nm AOT fraction FMF (open green circles), and fine-mode particle volume fraction FVF (multiplied by a factor of 5, open orange triangles) observed with AERONET sun/sky photometer. The measurements were performed at Ouarzazate (30.9° N, 6.9° W), very close to the Sahara in southeastern Morocco. Pure dust episodes occurred from 136–142 (16–21 May 2006) and from 154–159 (3–7 June 2006, indicated by vertical lines).

AMTD
7, 5173–5221, 2014

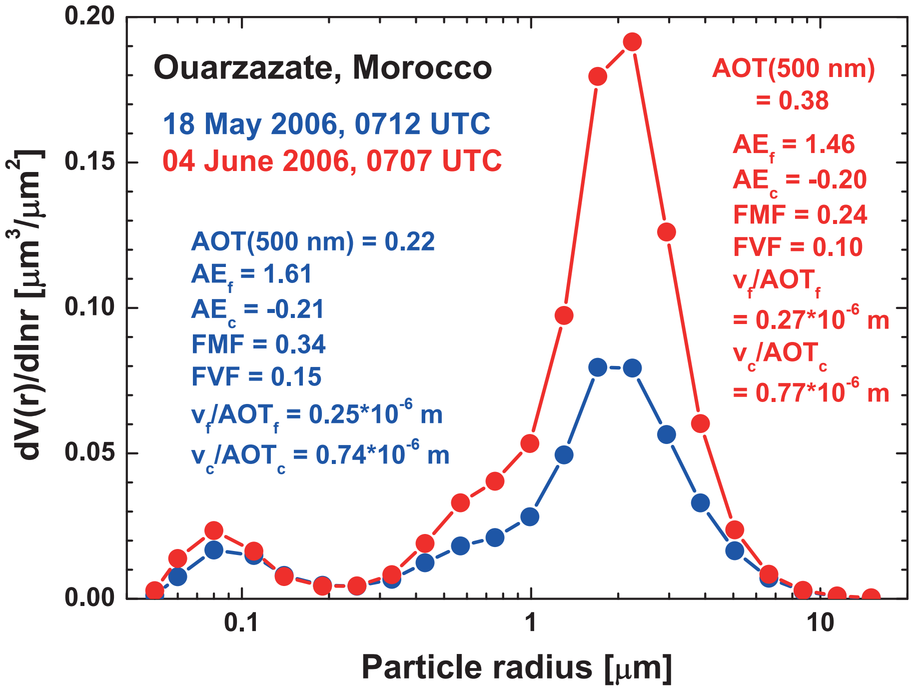

Figure 4. Column-integrated particle volume concentration as a function of particle radius (22 radius intervals) of pure Saharan dust observed with AERONET photometer over Ouarzazate, southern Morocco, during SAMUM-1 in the morning of 18 May 2006 (blue) and 4 June 2006 (red). Values for 500 nm AOT, fine-mode and coarse-mode Ångström exponents AE_f and AE_c, fine-mode fraction FMF, and fine-mode particle volume fraction FVF are given in addition. The conversion factors v_f/AOT_f and v_c/AOT_c for fine-mode and coarse-mode dust with volume fractions v_f and v_c, respectively, are used in the conversion of the lidar-derived optical properties into volume and mass concentrations by means of the POLIPHON method (see Sect. 4).

AMTD
7, 5173–5221, 2014

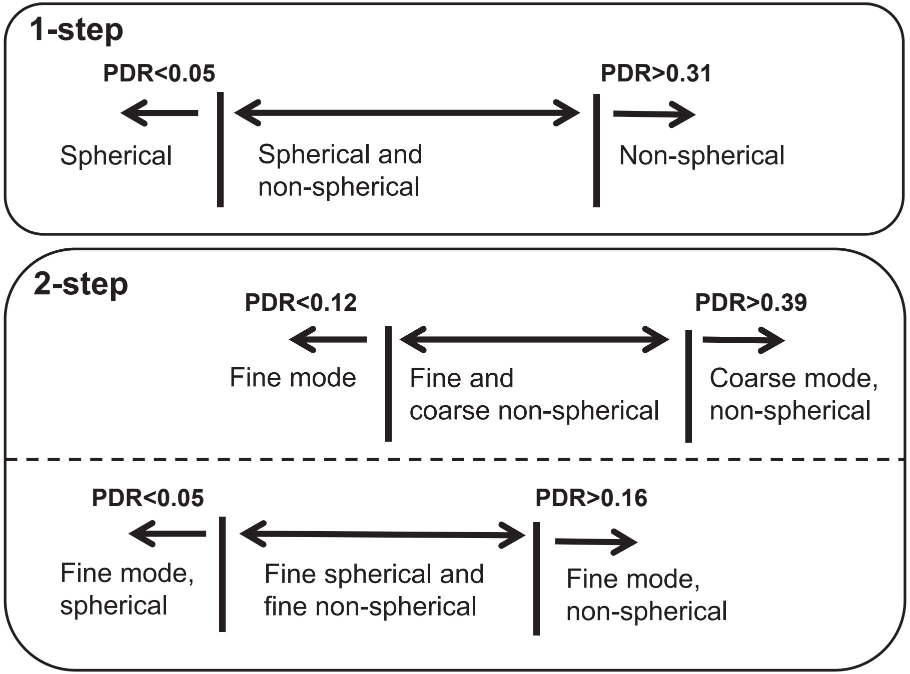

Figure 5. Illustration of the one-step and two-step methods to separate spherical particles from non-spherical dust particles (1-step method) and spherical particles (fine mode), fine dust, and coarse dust particles (two-step method) by means of particle depolarization ratio PDR.

AMTD
7, 5173–5221, 2014

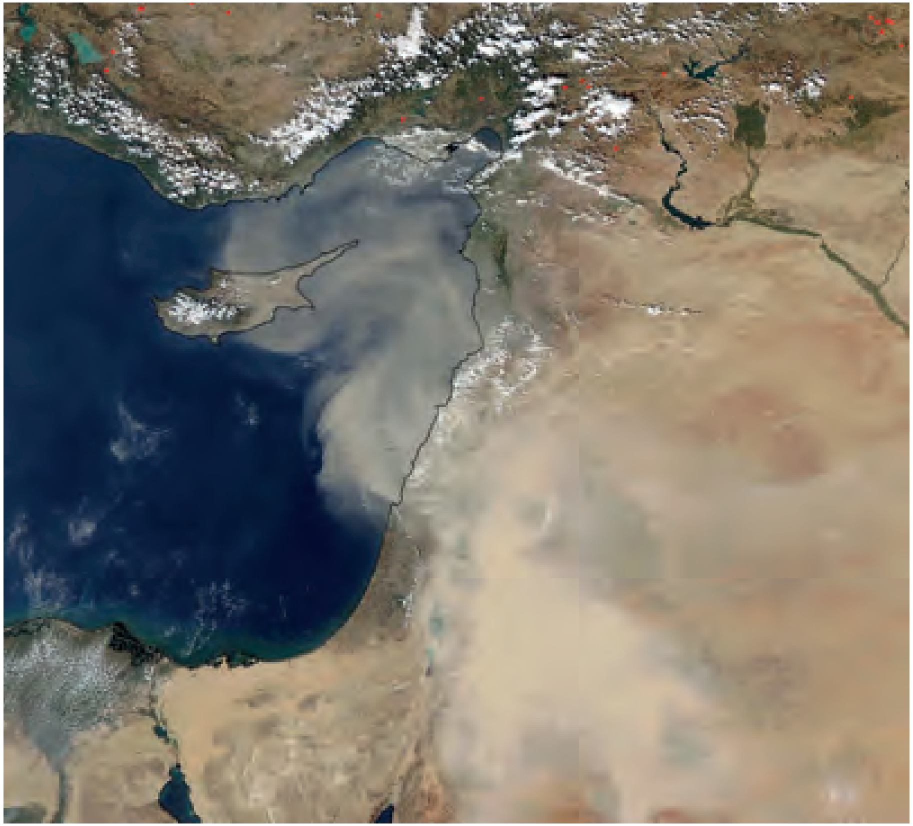

Figure 6. Dust outbreak from deserts in the Middle East reaching Cyprus on 28 September 2011 (TERRA-MODIS image, 08:30 UTC).

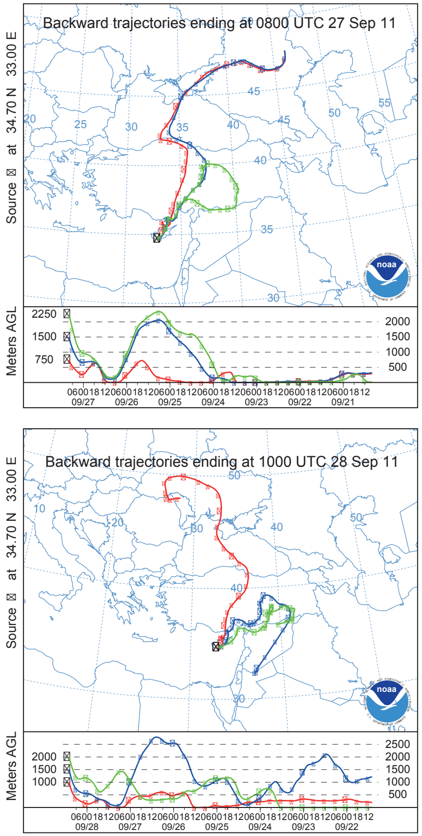

Figure 7. Seven-day backward trajectories arriving at Limassol, Cyprus, at different height levels (red, blue, green) on 27 September 2011, 08:00 UTC (top) and 28 September 2011, 10:00 UTC (bottom). Calculations are performed with HYSPLIT (HYbrid Single-Particle Lagrangian Integrated Trajectory) Model. Access via NOAA ARL READY Website (http://www.arl.noaa.gov/HYSPLIT.php).

AMTD
7, 5173–5221, 2014

R. E. Mamouri and A. Ansmann

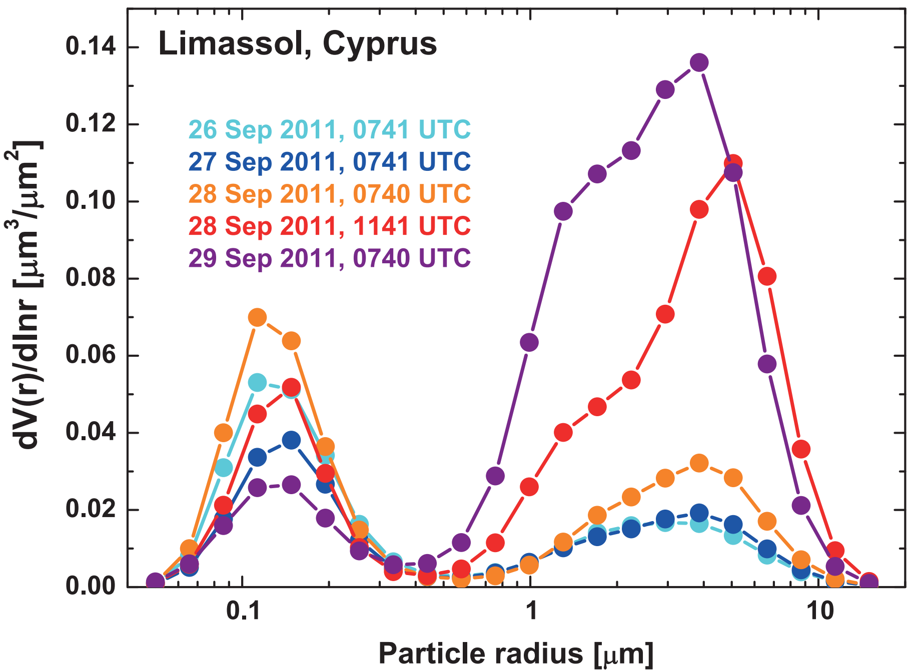

Figure 8. Column-integrated particle volume size distribution derived from AERONET sun/sky photometer observations at Limassol before (light blue and blue circles) and during the September 2011 dust outbreak (orange, red, purple circles).

AMTD
7, 5173–5221, 2014

Fine and coarse dust profiling

R. E. Mamouri and A. Ansmann

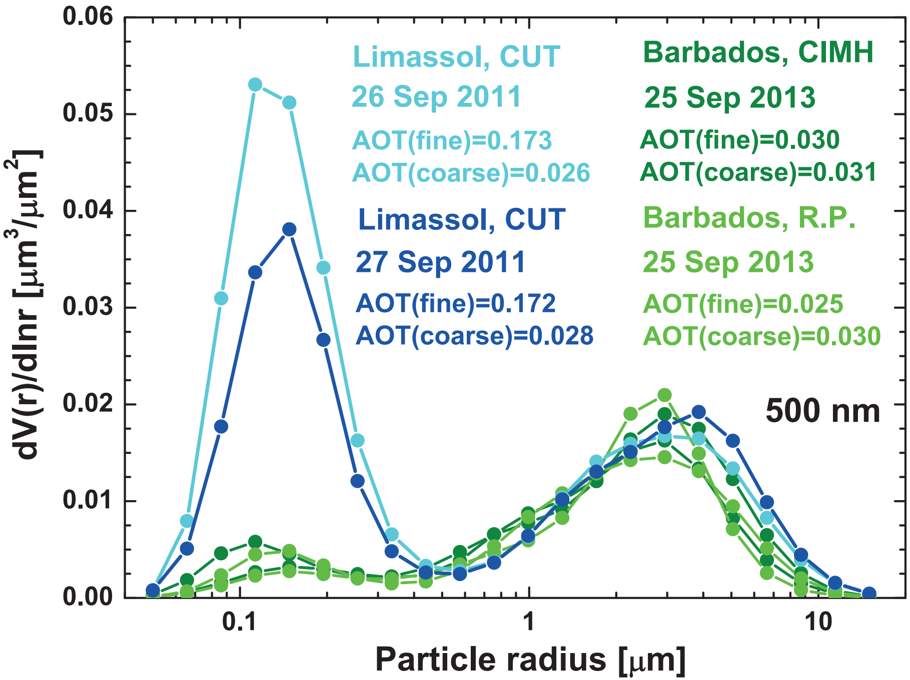

Figure 9. Column-integrated particle volume size distribution for pure marine conditions derived from AERONET observations at Barbados (CIMH and AERONET station Ragged Point, R. P.) on 25 September 2013 and for mixed aerosol conditions at the coastal AERONET station CUT, Limassol (measured at 07:41 UTC on 26 and 27 September 2011). The coarse mode at Limassol can be related to coarse marine particles. The pronounced fine mode is mostly related to urban haze in the boundary layer and fine-mode dust in the free troposphere.

AMTD
7, 5173–5221, 2014

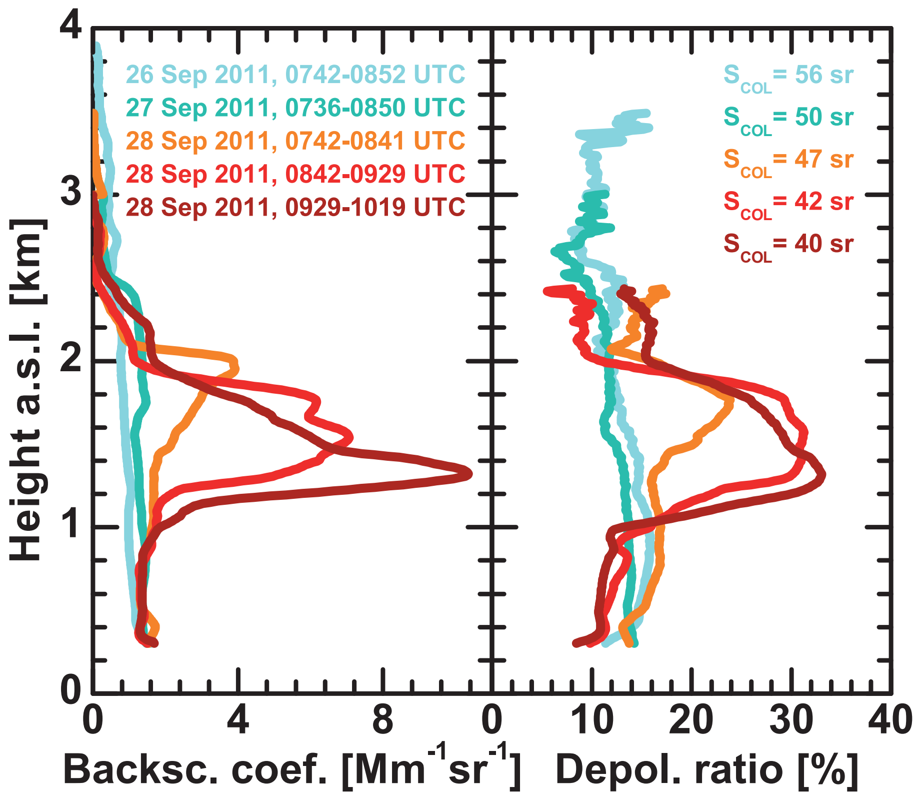

Figure 10. 532 nm particle backscatter coefficient (left) and particle linear depolarization ratio (right) in the free troposphere during a northerly airflow with fine-mode dust (26–27 September 2011) and during the arrival of a strong Arabian dust ourbreak in the morning of 28 September 2011. The column lidar ratios S_{col} for the entire vertical aerosol column are derived from combined photometer-lidar data analysis (Mamouri et al., 2013). 60–70 min of lidar return signals are averaged.

AMTD

7, 5173–5221, 2014

R. E. Mamouri and A. Ansmann

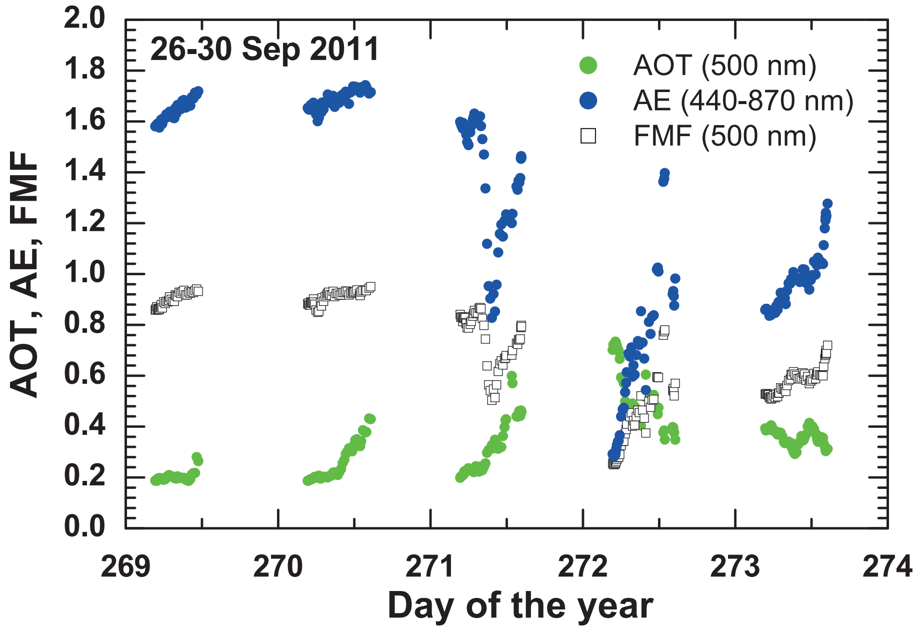

Figure 11. AERONET observations of 500 nm aerosol particle optical thickness (AOT), Ångström exponent (AE), and fine-mode fraction (FMF) for the 26–30 September 2011 period.

AMTD
7, 5173–5221, 2014

R. E. Mamouri and A. Ansmann

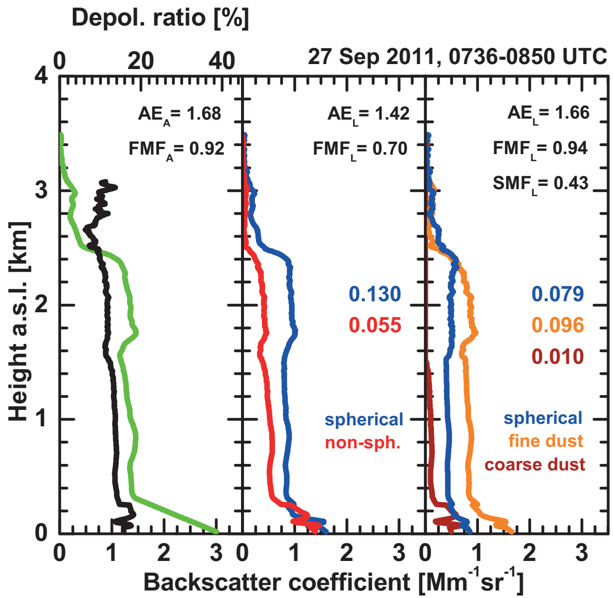

Figure 12. (Left) 532 nm particle backscatter coefficient (green) and particle linear depolarization ratio (black), (center) particle backscatter coefficient for non-spherical and spherical particles (1-step method), and (right) particle backscatter coefficient for spherical particles, fine and coarse dust (2-step method) observed on 29 September 2011, 07:36–08:50 UTC. 74 min of lidar return signals are thus averaged. The corresponding AOTs for the different aerosol components are given as colored numbers, computed from the backscatter profiles multiplied by approriate lidar ratios as given in Table 1. AE, FMF, and SMF denote Ångström exponent, fine-mode fraction, and spherical mode fraction, respectively. Index A indicates AERONET values, index L lidar-derived results obtained by means of Eqs. (22) and (23). In the central panel $FMF_L = SMF_L$. For the lowest 300 m a linear increase of the total backscatter coefficient from 300 m height to the surface (see left panel) is assumed.

AMTD
7, 5173–5221, 2014

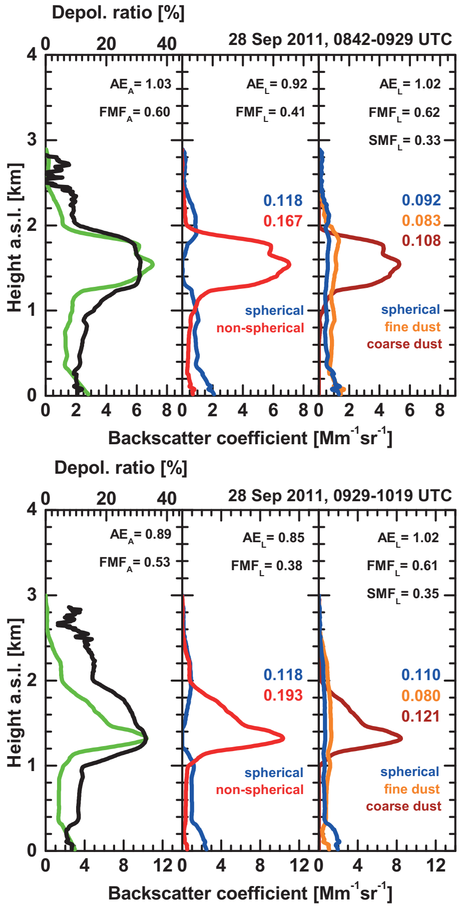

Figure 13. Same as Fig. 12, except for two periods on (top) 28 September 2011, 08:42–09:29 UTC (47 min signal average) and (bottom) 28 September 2011, 09:29–10:19 UTC (50 min signal average).

AMTD
7, 5173–5221, 2014

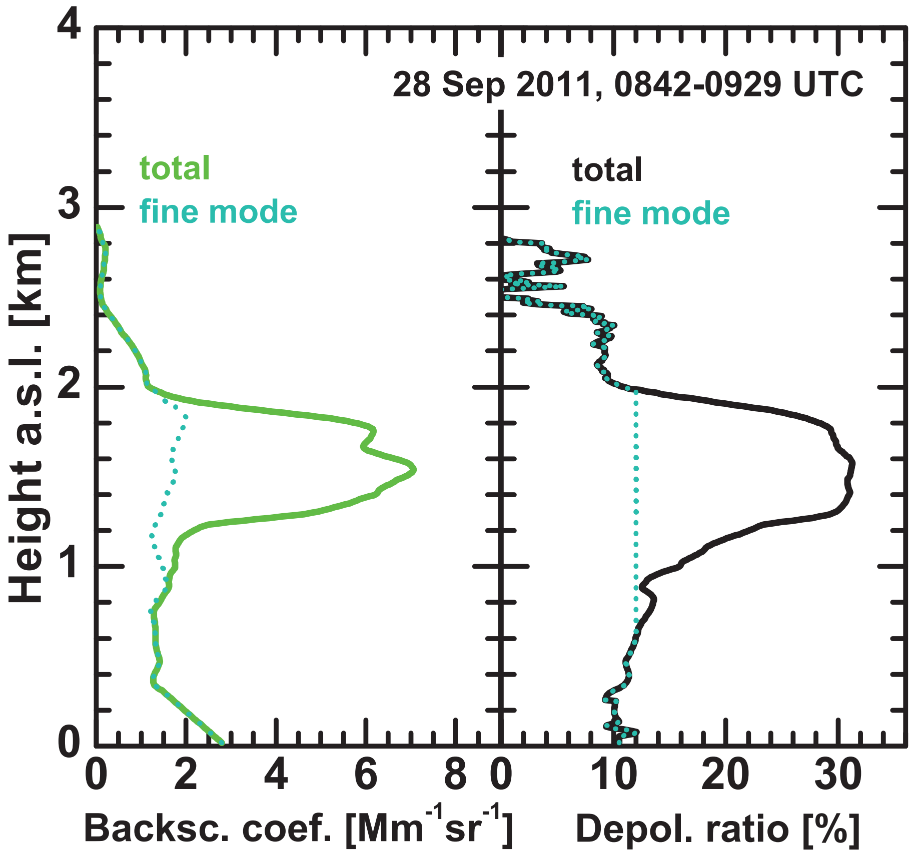

Figure 14. Total particle backscatter coefficient (green, left) and particle depolarization ratio (black, right) and respective fine-mode (fine sphercial particles and fine dust) contributions (blue dashed, obtained after step 1 of the 2-step data analysis). The fine-mode profiles are used as input for step 2 in the 2-step approach (see Fig. 5).

AMTD
7, 5173–5221, 2014

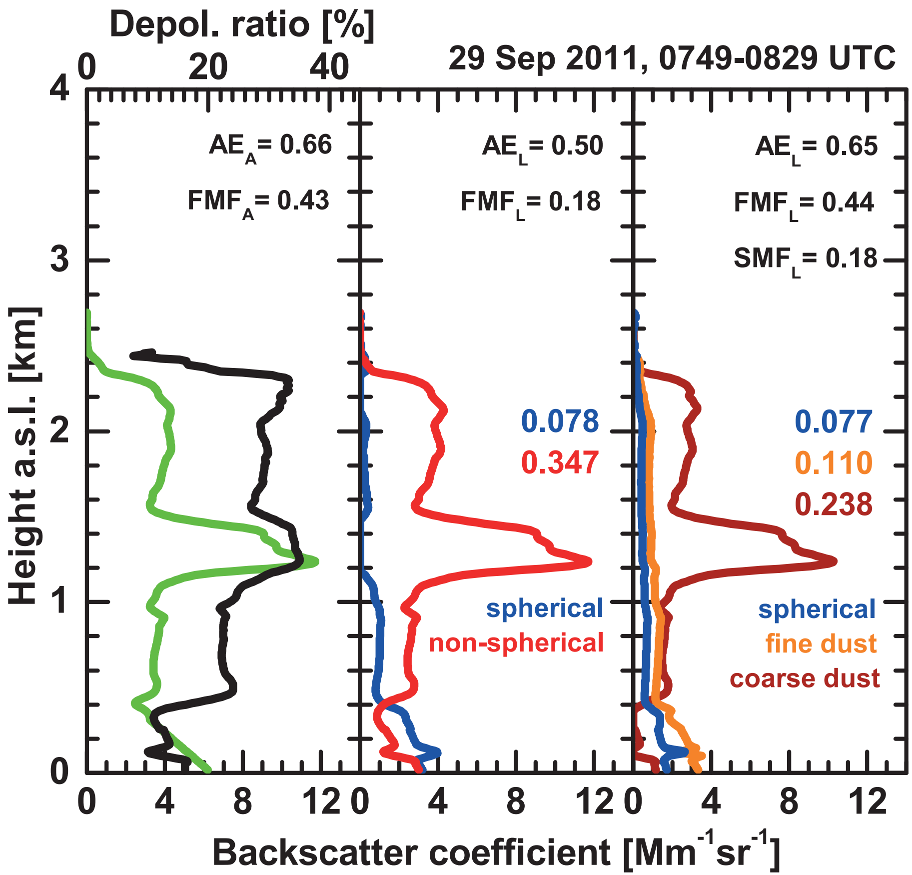

Figure 15. Same as Fig. 12, except for a morning measurement on 29 September 2011, 07:49–08:29 UTC (40 min signal average).

AMTD
7, 5173–5221, 2014

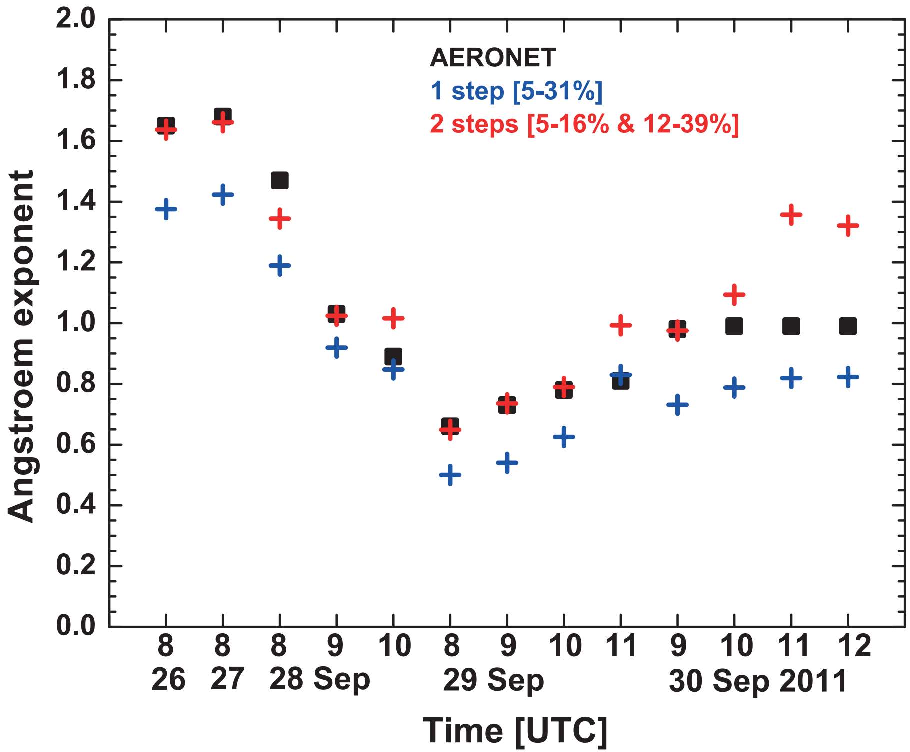

Figure 16. Comparison of Ångström exponents (AE_A vs. AE_L) derived from AERONET observations (black squares) and retrieved from the lidar measurements (blue crosses, 1-step method, red crosses, 2-step method) for the entire measurement period from 26–30 September 2011.

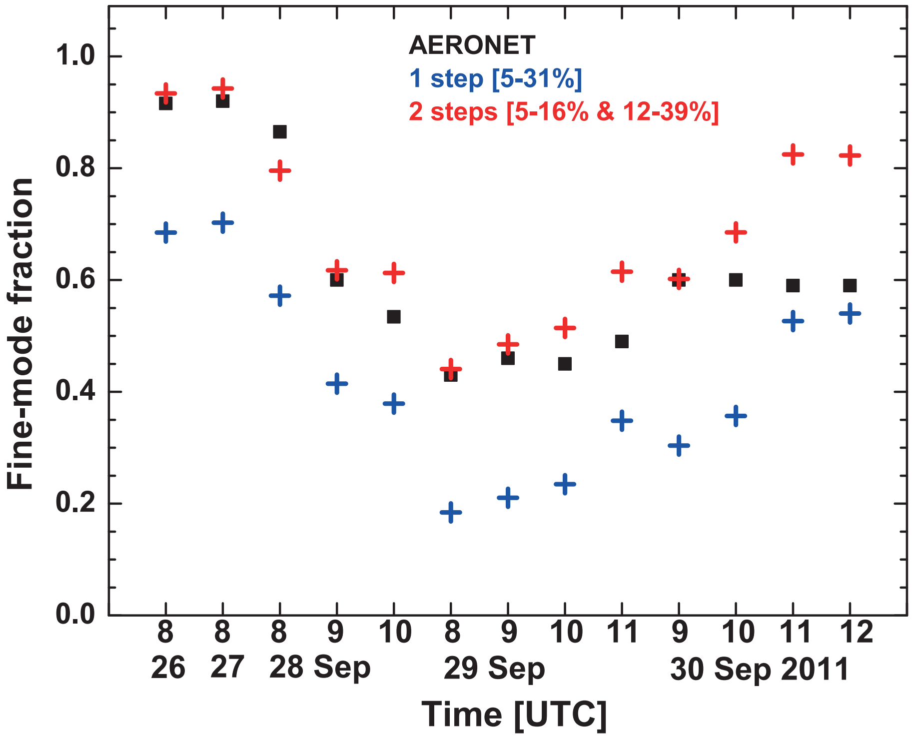

Figure 17. Same as Fig. 16, except for fine-mode fraction (FMF_A vs. FMF_L).

Discussion Paper | Discussion Paper | Discussion Paper | Discussion Paper |

AMTD
7, 5173–5221, 2014

Fine and coarse dust profiling

R. E. Mamouri and A. Ansmann

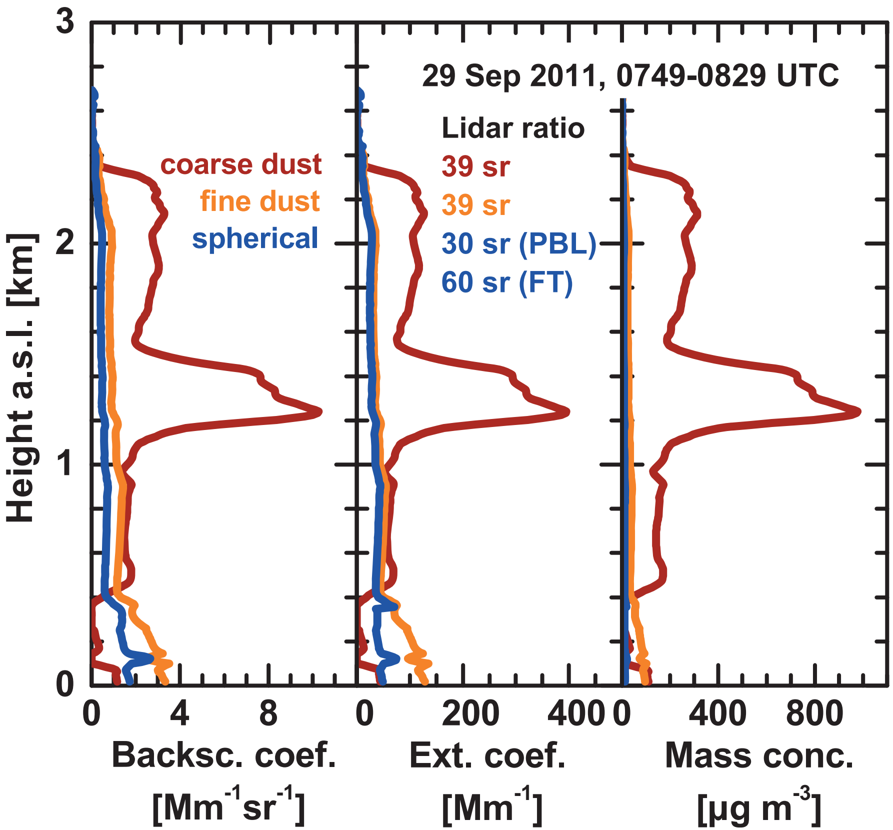

Figure 18. 532 nm particle backscatter and extinction coefficients, and particle mass concentrations computed from the backscatter coefficients in Fig. 15 by means of the two-step method, the lidar-ratio information in Table 1, and volume-to-extinction conversion factors as discussed in Sects. 3 and 4.

AMTD
7, 5173–5221, 2014

Fine and coarse dust profiling

R. E. Mamouri and A. Ansmann